7. Referências bibliográficas

1 SALUJA, R. K.; KUMAR, V.; SHAM, R. Stability of biodiesel–A review. **Renewable and Sustainable Energy Reviews,** v. 62, p. 866-881, 2016. ISSN 1364-0321.

2 13.263, L. D. P. D. R. N. **Lei da Presidência da República nº 13.263 de 23 de março de 2016, Diário Oficial da União de 24 de março de 2016.** 2016.

3 RODRIGUES, F. **Soja teve participação de 76,4% na produção de biodiesel em 2015, segundo dados da ANP**. Revista Biodieselbr 2016.

4 BIODIESELBR.COM, F. R.-. **Importações brasileiras de óleo diesel foram as menores em 6 anos**. BiodieselBR 2016.

5 MINISTÉRIO DA AGRICULTURA, P. E. A. S. E. C. G. D. A. À. C. S. E. T.-C. C. S. D. C. P. D. O. E. B. **Usos de biodiesel no Brasil e no mundo**. 2015

6 FERRARI, R. A.; OLIVEIRA, V. D. S.; SCABIO, A. Biodiesel de soja–taxa de conversão em ésteres etílicos, caracterização físico-química e consumo em gerador de energia. **Química Nova,** v. 28, n. 1, p. 19-23, 2005.

7 LORA, E. E. S. V., OSVALDO JOSÉ **Biocombustíveis**. 1. 2012. 202

8 VAN GERPEN, J. H. et al. Determining the influence of contaminants on biodiesel properties. **SAE paper,** v. 971685, 1997.

9 YAMANE, K. et al. Oxidation stability of biodiesel and its effects on diesel combustion and emission characteristics. **International Journal of Engine Research,** v. 8, n. 3, p. 307-319, 2007. ISSN 1468-0874.

10 DUNN, R. O. Effect of temperature on the oil stability index (OSI) of biodiesel. **Energy & Fuels,** v. 22, n. 1, p. 657-662, 2007. ISSN 0887-0624.

[11] DU PLESSIS, L.; DE VILLIERS, J.; VAN DER WALT, W. Stability studies on methyl and ethyl fatty acid esters of sunflowerseed oil. **Journal of the American Oil Chemists' Society,** v. 62, n. 4, p. 748-752, 1985. ISSN 0003-021X.

[12] MITTELBACH, M.; SCHOBER, S. The influence of antioxidants on the oxidation stability of biodiesel. **Journal of the American Oil Chemists' Society,** v. 80, n. 8, p. 817-823, 2003. ISSN 0003-021X.

[13] KNOTHE, G.; DUNN, R. O. Dependence of oil stability index of fatty compounds on their structure and concentration and presence of metals. **Journal of the American Oil Chemists' Society,** v. 80, n. 10, p. 1021-1026, 2003. ISSN 0003-021X.

[14] POLAVKA, J. et al. Oxidation stability of methyl esters studied by differential thermal analysis and Rancimat. **Journal of the American Oil Chemists' Society,** v. 82, n. 7, p. 519-524, 2005. ISSN 0003-021X.

[15] KNOTHE, G. Analyzing biodiesel: standards and other methods. **Journal of the American Oil Chemists' Society,** v. 83, n. 10, p. 823-833, 2006. ISSN 0003-021X.

[16] GONZAGA, F. B.; PASQUINI, C. A new method for determination of the oxidative stability of edible oils at frying temperatures using near infrared emission spectroscopy. **Analytica chimica acta,** v. 570, n. 1, p. 129-135, 2006. ISSN 0003-2670.

[17] KNOTHE, G. Some aspects of biodiesel oxidative stability. **Fuel Processing Technology,** v. 88, n. 7, p. 669-677, 2007. ISSN 0378-3820.

[18] MCCORMICK, R. et al. Several factors affecting the stability of biodiesel in standard accelerated tests. **Fuel Processing Technology,** v. 88, n. 7, p. 651-657, 2007. ISSN 0378-3820.

[19] DAS, L. et al. Long-term storage stability of biodiesel produced from Karanja oil. **Fuel,** v. 88, n. 11, p. 2315-2318, 2009. ISSN 0016-2361.

[20] BONDIOLI, P. et al. Biodiesel stability under commercial storage conditions over one year. **European Journal of Lipid Science and Technology,** v. 105, n. 12, p. 735-741, 2003. ISSN 1438-9312.

21 BOUAID, A.; MARTINEZ, M.; ARACIL, J. Long storage stability of biodiesel from vegetable and used frying oils. **Fuel,** v. 86, n. 16, p. 2596-2602, 2007. ISSN 0016-2361.

22 KNOTHE, G. Rapid monitoring of transesterification and assessing biodiesel fuel quality by near-infrared spectroscopy using a fiber-optic probe. **Journal of the American Oil Chemists' Society,** v. 76, n. 7, p. 795-800, 1999. ISSN 0003-021X.

23 KNOTHE, G. Monitoring a progressing transesterification reaction by fiber-optic near infrared spectroscopy with correlation to 1H nuclear magnetic resonance spectroscopy. **Journal of the American Oil Chemists' Society,** v. 77, n. 5, p. 489-493, 2000. ISSN 0003-021X.

24 ZAGONEL, G. F.; PERALTA-ZAMORA, P.; RAMOS, L. P. Multivariate monitoring of soybean oil ethanolysis by FTIR. **Talanta,** v. 63, n. 4, p. 1021-1025, 2004. ISSN 0039-9140.

25 ISMAIL, A. et al. Rapid quantitative determination of free fatty acids in fats and oils by Fourier transform infrared spectroscopy. **Journal of the American Oil Chemists' Society,** v. 70, n. 4, p. 335-341, 1993. ISSN 0003-021X.

26 DUBOIS, J. et al. Quantitative Fourier transform infrared analysis for anisidine value and aldehydes in thermally stressed oils. **Journal of the American Oil Chemists' Society,** v. 73, n. 6, p. 787-794, 1996. ISSN 0003-021X.

27 AL-ALAWI, A.; VAN DE VOORT, F. R.; SEDMAN, J. New FTIR method for the determination of FFA in oils. **Journal of the American Oil Chemists' Society,** v. 81, n. 5, p. 441-446, 2004. ISSN 0003-021X.

28 AL-ALAWI, A. et al. Automated FTIR analysis of free fatty acids or moisture in edible oils. **Journal of the Association for laboratory Automation,** v. 11, n. 1, p. 23-29, 2006. ISSN 2211-0682.

29 MAN, Y. C.; SETIOWATY, G. Determination of anisidine value in thermally oxidized palm olein by fourier transform infrared spectroscopy. **Journal of the American Oil Chemists' Society,** v. 76, n. 2, p. 243-247, 1999. ISSN 0003-021X.

30 MUNIATEGUI, S.; PASEIRO, P.; SIMAL, J. Medida del grado de insaturación de aceites y grasas comestibles por espectroscopia infrarroja y su relación con el índice de yodo. **Grasas Aceites,** v. 43, p. 1-5, 1992.

31 MAN, Y. C.; SETIOWATY, G.; VAN DE VOORT, F. Determination of iodine value of palm oil by Fourier transform infrared spectroscopy. **Journal of the American Oil Chemists' Society,** v. 76, n. 6, p. 693-699, 1999. ISSN 0003-021X.

32 HENDL, O. et al. A rapid and simple method for the determination of iodine values using derivative Fourier transform infrared measurements. **Analytica chimica acta,** v. 427, n. 1, p. 75-81, 2001. ISSN 0003-2670.

33 CANOIRA, L. et al. Biodiesel from low-grade animal fat: production process assessment and biodiesel properties characterization. **Industrial & Engineering Chemistry Research,** v. 47, n. 21, p. 7997-8004, 2008. ISSN 0888-5885.

34 GUARIEIRO, L. L. N. et al. Metodologia analítica para quantificar o teor de biodiesel na mistura biodiesel: diesel utilizando espectroscopia na região do infravermelho. **Quimica Nova,** v. 31, n. 2, p. 421-426, 2008.

35 ABNT, N. **ABNT NBR 15568:2008, Biodiesel - Determinação do teor de biodiesel em óleo diesel por espectroscopia na região do infravermelho médio**. Associação Brasileira de Normas Técnicas, Rio de Janeiro,< www. abnt. org. br 2008.

36 STANDARD, A. **ASTM D7371:2007. Standard test method for the determination of biodiesel (fatty acid methyl esters) content in diesel fuel oil using mid-infrared spectroscopy (FTIR-ATR-PLS method). West Conshohocken, PA: ASTM International; 2007** 2007.

37 STANDARDS, E. **DIN EN 14078:2014. Liquid petroleum products – Determination of fatty acid methyl ester (FAME) content in middle distillates – Infrared spectrometry method.** 2014.

38 DE SOUZA, A. V. A.; CAJAIBA DA SILVA, J. O. F. Biodiesel Synthesis Evaluated by Using Real-Time ATR-FTIR. **Organic Process Research & Development,** v. 17, n. 1, p. 127-132, 2012. ISSN 1083-6160.

39 GHESTI, G. F. et al. FT-Raman spectroscopy quantification of biodiesel in a progressive soybean oil transesterification reaction and its correlation

with 1H NMR spectroscopy methods. **Energy & Fuels,** v. 21, n. 5, p. 2475-2480, 2007. ISSN 0887-0624.

40 BRASIL, N. I. A., M. A. S.; SOUSA, E. C. M. . **Processamento de petróleo e gás**. 2012.

41 ANP. **Resolução ANP nº 50 de 23 Dezembro 2013, DOU de 24 Dezembro 2013.** 2013.

42 ANP. **Resolução ANP nº 13 de 06 Março 2015, DOU de 09 Março 2015.** 2015.

43 ANP. **Resolução ANP nº 69 de 23 Dezembro 2014, DOU de 24 Dezembro 2014.** 2014.

44 PETROBRAS. Características do óleo diesel. <http://www.br.com.br /wps/portal/portalconteudo/produtos/paraembarcacoes/oleodiesel/>. . 2012.

45 ROCHA, M. I.; GOMES, H. O. Óleo Diesel com Baixo Teor de Enxofre– Considerações quanto à Lubricidade e Condutividade Elétrica. **XVII Simpósio Internacional de Engenharia Automotiva–SIMEA**, 2009.

46 ANP. **Orientações e Procedimentos para o Manuseio e Armazenagem de Óleo Diesel B** 2010.

47 ANP. **Resolução ANP nº 45 de 25 Agosto 2014, DOU de 26 Agosto 2014.** 2014.

48 KNOTHE, G. et al. Manual de Biodiesel Edgard Blücher. **São Paulo**, 2006.

49 GERIS, R. et al. Biodiesel de soja-reação de transesterificação para aulas práticas de química orgânica. **Química Nova,** v. 30, n. 5, p. 1369, 2007. ISSN 0100-4042.

50 RAMOS, L. et al. Tecnologias de Produção de Biodiesel Ramos, LP. 2011.

51 LUTTERBACH, M. T.; GALVÃO, M. M. Fuel for the future: biodiesel–a case study. In: (Ed.). **Applied Microbiology and Molecular Biology in Oilfield Systems**: Springer, 2010. p.229-235. ISBN 904819251X.

52 CAVALCANTI, E. H. D. S. **Estudo da Vida de Prateleira de Biodiesel, Blendas e Misturas em Tanques de Armazenamento Simulado**: INT 2013.

53 JAIN, S.; SHARMA, M. Stability of biodiesel and its blends: a review. **Renewable and Sustainable Energy Reviews,** v. 14, n. 2, p. 667-678, 2010. ISSN 1364-0321.

54 MUSHRUSH, G. W. et al. Fuel Instability Studies: The Chemical Validation of ASTM Method D5304. **Petroleum science and technology,** v. 19, n. 5-6, p. 561-572, 2001. ISSN 1091-6466.

55 CANDEIA, R. et al. Influence of the storage on the thermo-oxidative stability of methyl and ethyl esters by PDSC. **Journal of thermal analysis and calorimetry,** v. 106, n. 2, p. 581-586, 2011. ISSN 1388-6150.

56 KAMAL-ELDIN, A.; POKORNY, J. Lipid oxidation products and methods used for their analysis. **Analysis of lipid oxidation. Champaign: AOCS**, 2005.

57 DUNN, R. O. Oxidative stability of biodiesel by dynamic mode pressurized-differential scanning calorimetry (P-DSC). **Transactions of the ASABE,** v. 49, n. 5, p. 1633-1641, 2006.

58 DE MORAES CINI, J. R. et al. Comparação dos métodos de determinação da estabilidade oxidativa de biodiesel B100, em mistura com antioxidantes sintéticos. Aplicação do delineamento simplex-centroide com variável de processo. **Quim. Nova,** v. 36, n. 1, p. 79-84, 2013.

59 ABNT, N. **ABNT NBR 15512:2014, Biodiesel - Armazenamento, transporte, abastecimento e controle de qualidade de biodiesel e/ou óleo diesel BX**. Associação Brasileira de Normas Técnicas, Rio de Janeiro,< www. abnt. org. br 2014.

60 LÔBO, I. P.; FERREIRA, S. L. C.; CRUZ, R. S. D. Biodiesel: parâmetros de qualidade e métodos analíticos. 2009. ISSN 0100-4042.

61 BORSATO, D. et al. Aplicação do delineamento simplex-centroide no estudo da cinética da oxidação de Biodiesel B100 em mistura com antioxidantes sintéticos. **Quim. Nova,** v. 33, n. 8, p. 1726-1731, 2010.

62 LIANG, Y. C. et al. The effect of natural and synthetic antioxidants on the oxidative stability of palm diesel. **Fuel,** v. 85, n. 5, p. 867-870, 2006. ISSN 0016-2361.

63 TANG, H. et al. Effect of antioxidants on the storage stability of soybean-oil-based biodiesel. **Energy & Fuels,** v. 24, n. 3, p. 2028-2033, 2009. ISSN 0887-0624.

64 SANTOS, F. F. P. D. **Avaliação de antioxidantes aplicados à produção de biodiesel**. 2013.

65 DAMASCENO, S. S. Avaliação da atividade antioxidante dos ácidos caféico e ferúlico no controle da estabilidade oxidativa do biodiesel de soja. 2011.

66 DE OLIVEIRA FILHO, W. P. **Utilização de cromatografia gasosa para a determinação de antioxidantes sintéticos em biodiesel: uma abordagem metrológica**. 2013. (Tese de Doutorado). Universidade de São Paulo

67 RAMALHO, V. C.; JORGE, N. Antioxidantes utilizados em óleos, gorduras e alimentos gordurosos. **Química Nova,** v. 29, n. 4, p. 755, 2006. ISSN 0100-4042.

68 FRANKEL, E. N. Lipid oxidation. **Progress in lipid research,** v. 19, n. 1, p. 1-22, 1980. ISSN 0163-7827.

69 STANDARD, A. **ASTM D4625:2009. Standard Test Method for Middle Distillate Fuel Storage Stability at 43 °C (110 °F).** 2009.

70 STANDARDS, E. **DIN EN 15751:2014. Automotive fuels – fatty acid methyl ester (FAME) fuel and blends with diesel fuel – Determination of oxidation stability by accelerated oxidation method.** 2014.

71 STANDARD, A. **ASTM D6304:2007. Standard Test Method for Determination of Water in Petroleum Products, Lubricating Oils, and Additives by Coulometric Karl Fischer Titration** 2007.

72 STANDARD, A. **ASTM D664:2011. Standard test method for acid number of petroleum products by potentiometric titration.** 2011.

73 STANDARD, A. **ASTM D7111:2015. Standard Test Method for Determination of Trace Elements in Middle Distillate Fuels by Inductively Coupled Plasma Atomic Emission Spectrometry (ICP-AES)** 2015.

74 ABNT, N. **ABNT NBR 15553:2015, Biodiesel - Determinação dos teores de cálcio, magnésio, sódio, fósforo e potássio por espectrometria de emissão ótica com plasma indutivamente acoplado (ICPOES).** Associação Brasileira de Normas Técnicas, Rio de Janeiro,< www. abnt. org. br 2015.

75 STANDARDS, E. **DIN EN 14111:2003-10. Fat and oil derivatives - Fatty acid methyl esters (FAME) - Determination of iodine value.** 2003.

76 RODRIGUES, J. et al. Water content determination in biodiesel: optimization of methodology in coulometric Karl Fischer titration. **Journal of ASTM International,** v. 7, n. 2, p. 1-7, 2009. ISSN 1546-962X.

77 FREGOLENTE, P. B. L.; FREGOLENTE, L. V.; WOLF MACIEL, M. R. Water content in biodiesel, diesel, and biodiesel–diesel blends. **Journal of chemical & engineering data,** v. 57, n. 6, p. 1817-1821, 2012. ISSN 0021-9568.

78 MILLER, J. N.; MILLER, J. C. **Statistics and chemometrics for analytical chemistry**. Pearson Education, 2005. ISBN 0131291920.

79 DE SOUSA, L. S. et al. Use of natural antioxidants in soybean biodiesel. **Fuel,** v. 134, p. 420-428, 2014. ISSN 0016-2361.

80 EL BOULIFI, N. et al. Process optimization for biodiesel production from corn oil and its oxidative stability. **International Journal of Chemical Engineering,** v. 2010, 2010. ISSN 1687-806X.

81 CARVALHO, R. A. **Estudo da Adição de Biodiesel no Diesel S10 e S500 e seus Efeitos nas Propriedades do Combustível e na Atomização** 2015. Universidade Federal do Rio de Janeiro

82 ANP. **Resolução ANP nº 2 de 12 Janeiro 2011, DOU de 13 Janeiro 2011, recertificada no DOU 03 Fevereiro 2011.** 2011.

83 BONDIOLI, P. et al. The prediction of biodiesel storage stability. Proposal for a quick test. **European journal of lipid science and technology,** v. 106, n. 12, p. 822-830, 2004. ISSN 1438-9312.

84 GUILLÉN, M. D.; CABO, N. Infrared spectroscopy in the study of edible oils and fats. **Journal of the Science of Food and Agriculture,** v. 75, n. 1, p. 1-11, 1997. ISSN 1097-0010.

85 VAN DE VOORT, F.; ISMAIL, A.; SEDMAN, J. A rapid, automated method for the determination ofcis andtrans content of fats and oils by fourier transform infrared spectroscopy. **Journal of the American Oil Chemists' Society,** v. 72, n. 8, p. 873-880, 1995. ISSN 0003-021X.

86 SAFAR, M. et al. Characterization of edible oils, butters and margarines by Fourier transform infrared spectroscopy with attenuated total reflectance. **Journal of the American Oil Chemists' Society,** v. 71, n. 4, p. 371-377, 1994. ISSN 0003-021X.

87 GUILLÉN, M. D.; CABO, N. Some of the most significant changes in the Fourier transform infrared spectra of edible oils under oxidative conditions. **Journal of the Science of Food and Agriculture,** v. 80, n. 14, p. 2028-2036, 2000. ISSN 1097-0010.

88 OSAWA, W. et al. Effects of antioxidants on oxidation and storage stability of Croton megalocarpus biodiesel. **International Journal of Energy and Environmental Engineering**, p. 1-7, 2015. ISSN 2008-9163.

89 SCHNEIDER, C. An update on products and mechanisms of lipid peroxidation. **Molecular nutrition & food research,** v. 53, n. 3, p. 315-321, 2009. ISSN 1613-4133.

90 ARNOLD, R.; HARTUNG, T. Infrared spectroscopic determination of degree of unsaturation of fats and oils. **Journal of food science,** v. 36, n. 1, p. 166-168, 1971. ISSN 1750-3841.

[91] AFRAN, A.; NEWBERY, J. Analysis of the degree of unsaturation in edible oils by Fourier transform-infrared/attenuated total reflectance spectroscopy. **Spectroscopy,** v. 6, n. 1, p. 31-34, 1991.

[92] MORENO, M. M. et al. Determination of unsaturation grade and trans isomers generated during thermal oxidation of edible oils and fats by FTIR. **Journal of Molecular Structure,** v. 482, p. 551-556, 1999. ISSN 0022-2860.

[93] GUILLEN, M.; CABO, N. Characterization of edible oils and lard by Fourier transform infrared spectroscopy. Relationships between composition and frequency of concrete bands in the fingerprint region. **Journal of the American Oil Chemists' Society,** v. 74, n. 10, p. 1281-1286, 1997. ISSN 0003-021X.

[94] CHOE, E.; MIN, D. B. Mechanisms and factors for edible oil oxidation. **Comprehensive reviews in food science and food safety,** v. 5, n. 4, p. 169-186, 2006. ISSN 1541-4337.

[95] VIEIRA, A. D. S. **Influência do cobre (0) e cobre (II) sobre a degradação de óleos de canola e de girassol submetidos a estresse térmico**. 2015. 139 Química, PUC-Rio

[96] SILVERSTEIN, R. M. W., F. X. . **Spectrometric Identification of Organics Compounds**. Sixth. 1997.

[97] OLIVEIRA, F. C. et al. Adulteration of diesel/biodiesel blends by vegetable oil as determined by Fourier transform (FT) near infrared spectrometry and FT-Raman spectroscopy. **Analytica Chimica Acta,** v. 587, n. 2, p. 194-199, 2007. ISSN 0003-2670.

8. Anexos

Tabela A.1. Resultados com a média dos resultados de ICP OES das amostras estudadas no tempo inicial (t_0) e final (t_{24}).

Resultados ICP OES (mg kg^{-1})	**Sn**	**Cd**	**Zn**	**Cu**	**Pb**	**P**	**Ni**	**Na**	**Mg**	**K**	**Fe**	**Cr**	**Ca**
B100 - t_0	< 0.03	< 0.001	< 0.003	< 0.006	< 0.02	< 0.1	< 0.005	0.82	0.015	< 0.1	< 0.002	< 0.001	0.11
B100 - t_{24}	< 0.03	< 0.001	< 0.003	< 0.006	< 0.02	< 0.1	< 0.005	0.93	< 0.003	< 0.1	< 0.002	< 0.001	< 0.02
B20 S10 - t_0	< 0.03	< 0.001	< 0.003	< 0.006	< 0.02	< 0.1	< 0.005	1.6	0.034	< 0.1	< 0.002	< 0.001	0.10
B20 S10 - t_{24}	< 0.03	< 0.001	< 0.003	< 0.006	< 0.02	< 0.1	< 0.005	0.89	0.011	< 0.1	< 0.002	< 0.001	0.12
B20 S500 - t_0	< 0.03	< 0.001	< 0.003	< 0.006	< 0.02	< 0.03	< 0.005	< 0.1	< 0.003	< 0.1	< 0.002	< 0.001	0.14
B20 S500 - t_{24}	< 0.03	< 0.001	< 0.003	< 0.006	< 0.02	< 0.03	< 0.005	< 0.1	< 0.003	< 0.1	< 0.002	< 0.001	< 0.02
B7 S10 - t_0	< 0.03	< 0.001	< 0.003	< 0.006	< 0.02	< 0.1	< 0.005	1.01	0.027	< 0.1	< 0.002	< 0.001	0.040
B7 S10 - t_{24}	< 0.03	< 0.001	< 0.003	< 0.006	< 0.02	< 0.1	< 0.005	1.88	0.031	< 0.1	< 0.002	< 0.001	0.31
B7 S500 - t_0	< 0.03	< 0.001	< 0.003	< 0.006	< 0.02	< 0.03	< 0.005	< 0.1	< 0.003	< 0.1	< 0.002	< 0.001	0.13
B7 S500 - t_{24}	< 0.03	< 0.001	< 0.003	< 0.006	< 0.02	< 0.03	< 0.005	< 0.1	< 0.003	< 0.1	< 0.002	< 0.001	0.12
B0 S10 - t_0	< 0.03	< 0.001	< 0.003	< 0.006	< 0.02	< 0.1	< 0.005	0.56	< 0.003	< 0.1	< 0.002	< 0.001	< 0.02
B0 S10 - t_{24}	< 0.03	< 0.001	< 0.003	< 0.006	< 0.02	< 0.1	< 0.005	0.68	< 0.003	< 0.1	< 0.002	< 0.001	< 0.02
B0 S50 - t_0	< 0.03	< 0.001	< 0.003	< 0.006	< 0.02	< 0.1	< 0.005	1.1	0.022	< 0.1	< 0.002	< 0.001	0.48
B0 S500 - t_{24}	< 0.03	< 0.001	< 0.003	< 0.006	< 0.02	< 0.1	< 0.005	< 0.1	< 0.003	< 0.1	< 0.002	< 0.001	0.06

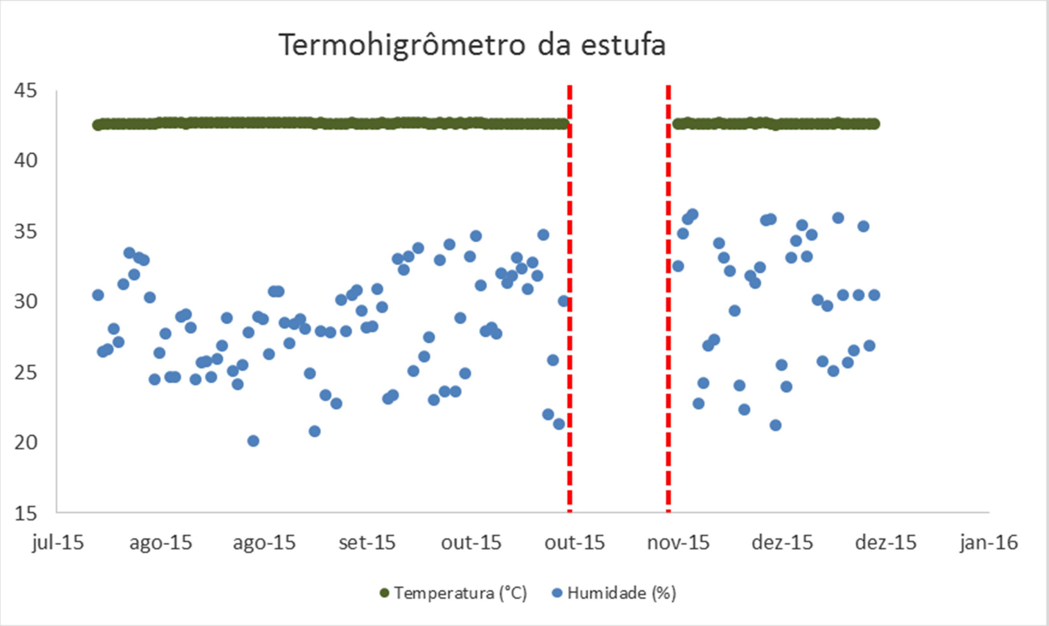

Figura A.1. Gráfico da temperatura e umidade do termohigrômetro em função do tempo. No intervalo entre 22-out-15 a 11-nov-15 a bateria do termohigrômetro acabou e ficou sem realizar as medidas.

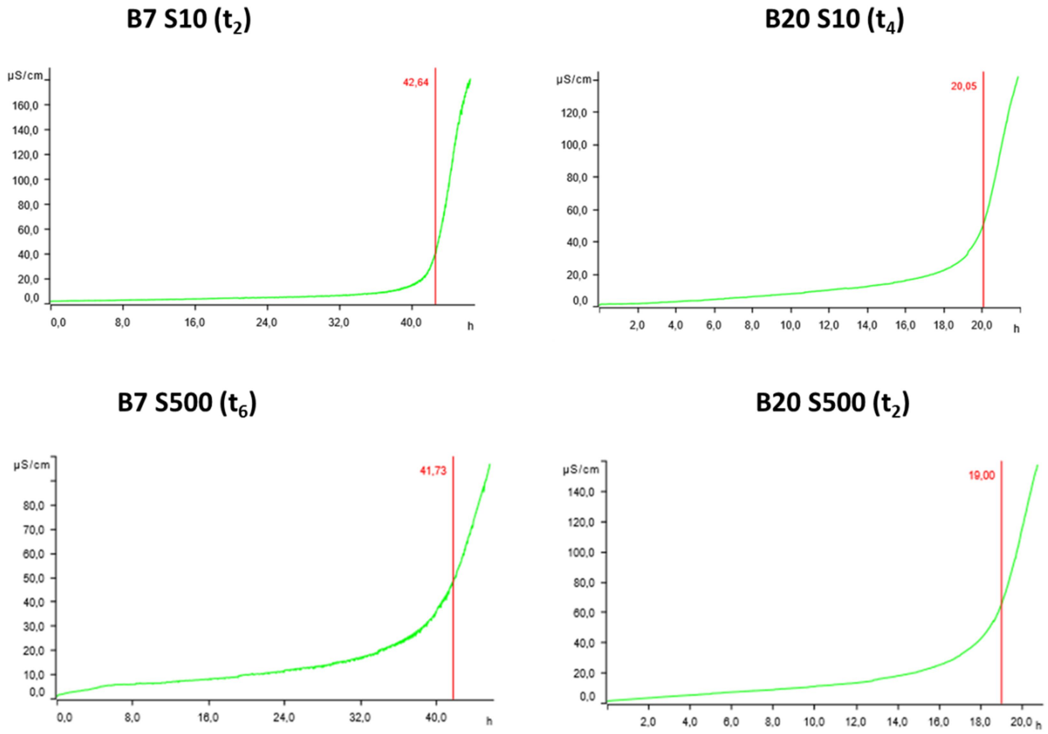

Figura A.2. Exemplos dos perfis das curvas do Rancimat® de condutividade elétrica *versus* tempo para os quatro tipos de misturas B7 S10, B20 S10, B7 S500 e B20 S500 em diferentes tempos.

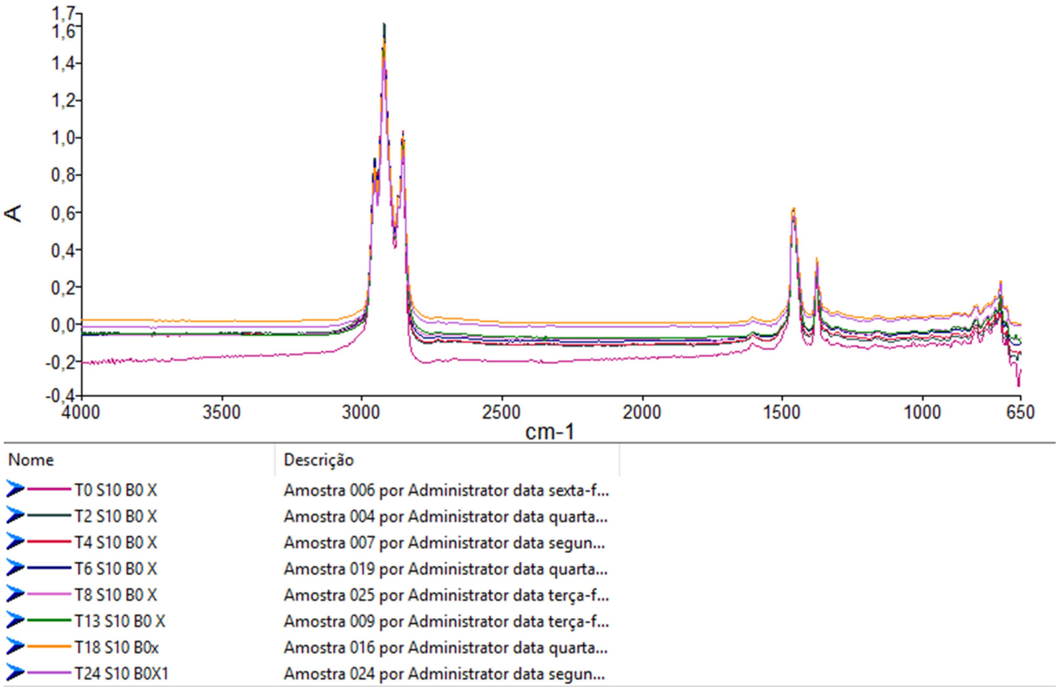

Nome	Descrição
T0 S10 B0 X	Amostra 006 por Administrator data sexta-f...
T2 S10 B0 X	Amostra 004 por Administrator data quarta...
T4 S10 B0 X	Amostra 007 por Administrator data segun...
T6 S10 B0 X	Amostra 019 por Administrator data quarta...
T8 S10 B0 X	Amostra 025 por Administrator data terça-f...
T13 S10 B0 X	Amostra 009 por Administrator data terça-f...
T18 S10 B0x	Amostra 016 por Administrator data quarta...
T24 S10 B0X1	Amostra 024 por Administrator data segun...

Figura A.3. Espectros comparativos de FTIR-HATR da mistura B0 S10 (replicatas x) nos tempos 0, 2, 4, 6, 8, 13, 18 e 24 semanas de envelhecimento a 43 °C.

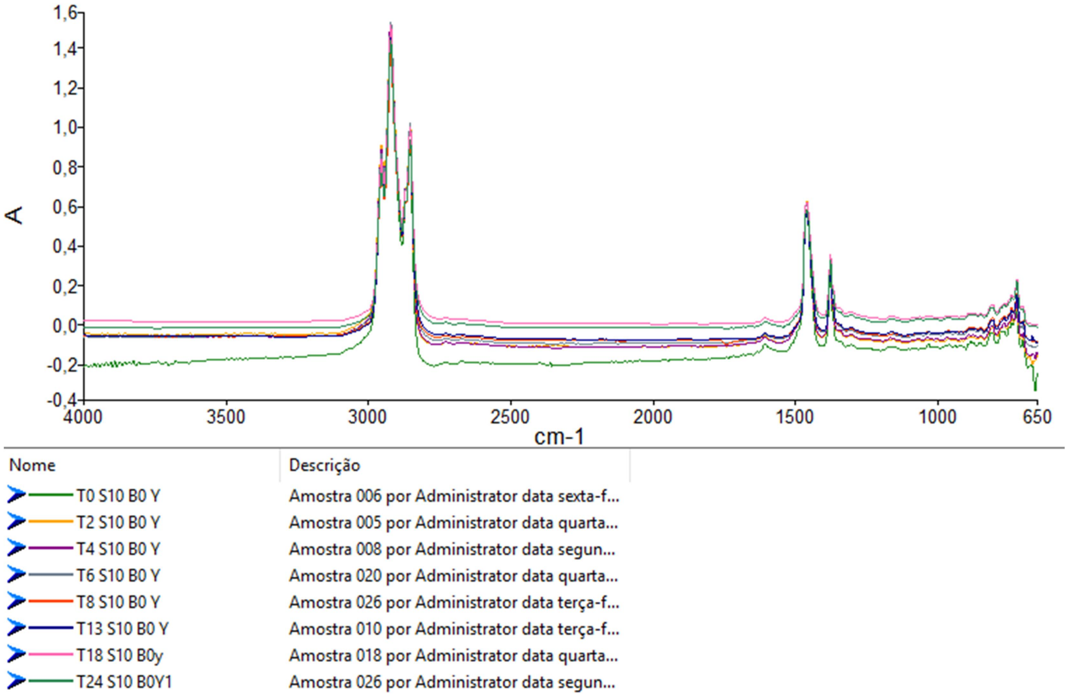

Nome	Descrição
T0 S10 B0 Y	Amostra 006 por Administrator data sexta-f...
T2 S10 B0 Y	Amostra 005 por Administrator data quarta...
T4 S10 B0 Y	Amostra 008 por Administrator data segun...
T6 S10 B0 Y	Amostra 020 por Administrator data quarta...
T8 S10 B0 Y	Amostra 026 por Administrator data terça-f...
T13 S10 B0 Y	Amostra 010 por Administrator data terça-f...
T18 S10 B0y	Amostra 018 por Administrator data quarta...
T24 S10 B0Y1	Amostra 026 por Administrator data segun...

Figura A.4. Espectros comparativos de FTIR-HATR da mistura B0 S10 (replicatas y) nos tempos 0, 2, 4, 6, 8, 13, 18 e 24 semanas de envelhecimento a 43 °C.

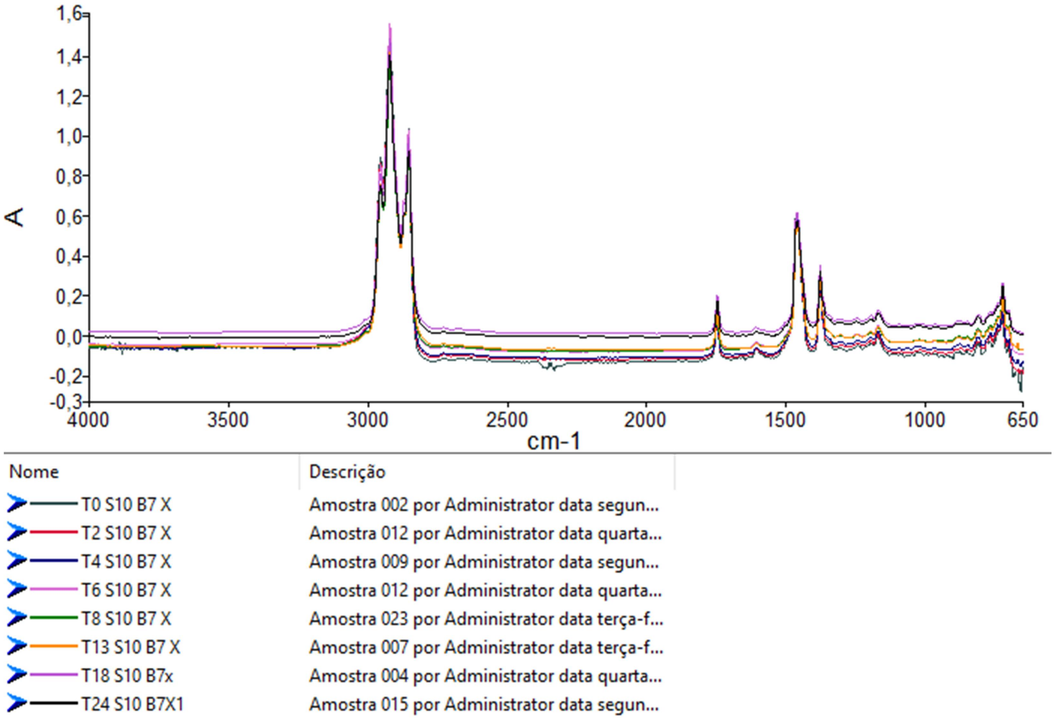

Nome	Descrição
T0 S10 B7 X	Amostra 002 por Administrator data segun...
T2 S10 B7 X	Amostra 012 por Administrator data quarta...
T4 S10 B7 X	Amostra 009 por Administrator data segun...
T6 S10 B7 X	Amostra 012 por Administrator data quarta...
T8 S10 B7 X	Amostra 023 por Administrator data terça-f...
T13 S10 B7 X	Amostra 007 por Administrator data terça-f...
T18 S10 B7x	Amostra 004 por Administrator data quarta...
T24 S10 B7X1	Amostra 015 por Administrator data segun...

Figura A.5. Espectros comparativos de FTIR-HATR da mistura B7 S10 (replicatas x) nos tempos 0, 2, 4, 6, 8, 13, 18 e 24 semanas de envelhecimento a 43 °C.

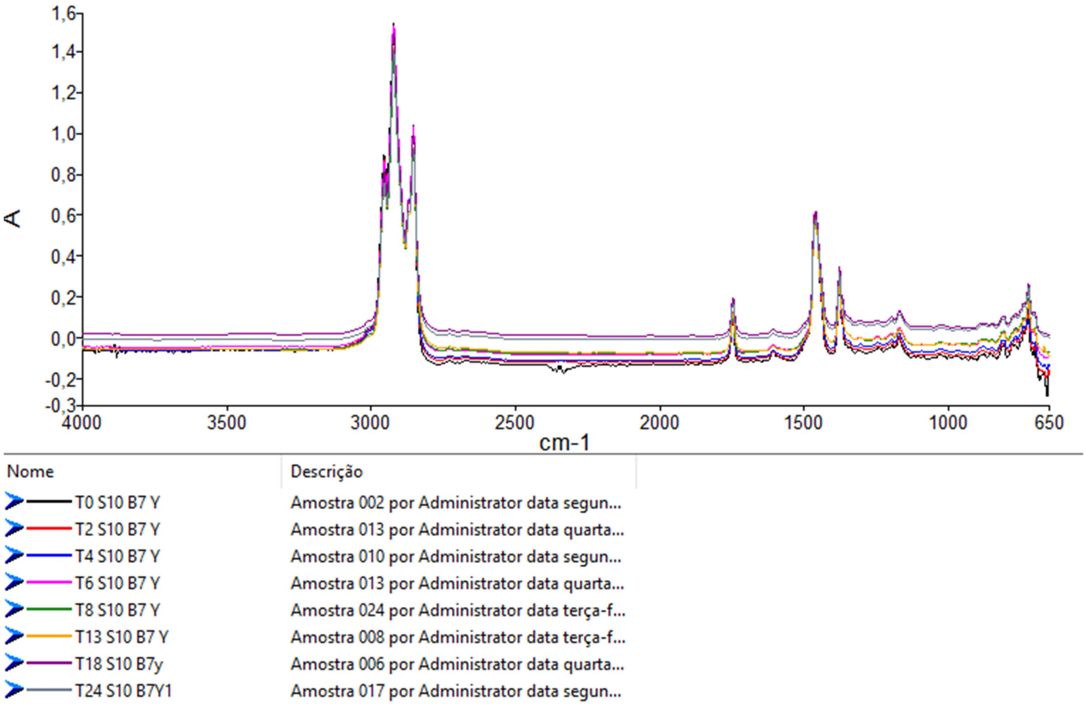

Nome	Descrição
T0 S10 B7 Y	Amostra 002 por Administrator data segun...
T2 S10 B7 Y	Amostra 013 por Administrator data quarta...
T4 S10 B7 Y	Amostra 010 por Administrator data segun...
T6 S10 B7 Y	Amostra 013 por Administrator data quarta...
T8 S10 B7 Y	Amostra 024 por Administrator data terça-f...
T13 S10 B7 Y	Amostra 008 por Administrator data terça-f...
T18 S10 B7y	Amostra 006 por Administrator data quarta...
T24 S10 B7Y1	Amostra 017 por Administrator data segun...

Figura A.6. Espectros comparativos de FTIR-HATR da mistura B7 S10 (replicatas y) nos tempos 0, 2, 4, 6, 8, 13, 18 e 24 semanas de envelhecimento a 43 °C.

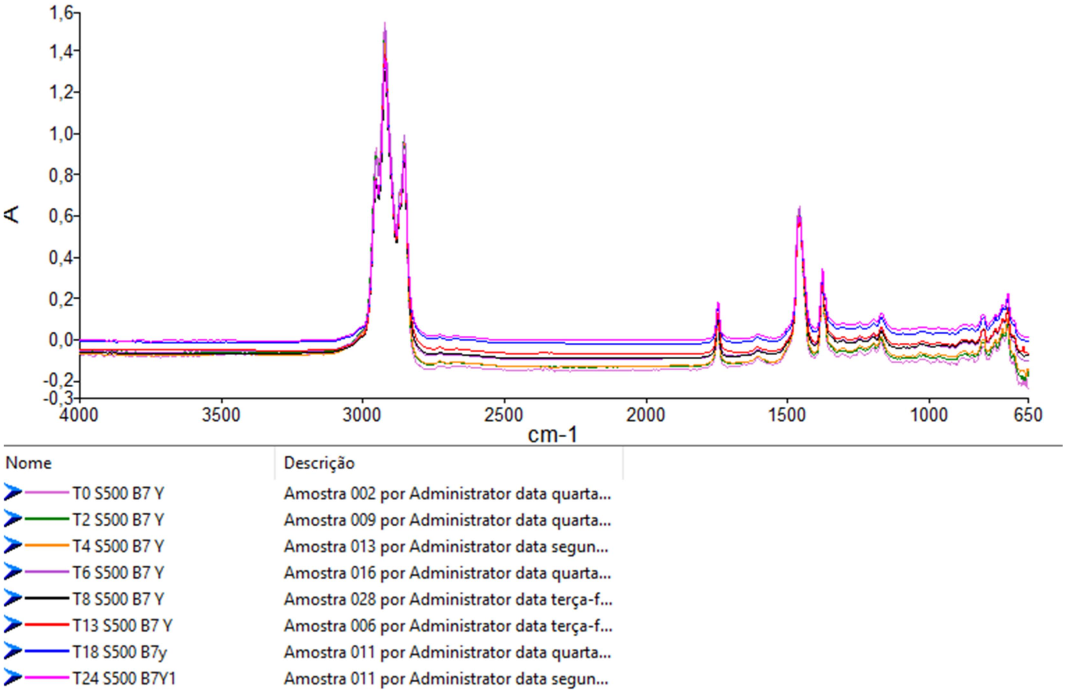

Nome	Descrição
T0 S500 B7 Y	Amostra 002 por Administrator data quarta...
T2 S500 B7 Y	Amostra 009 por Administrator data quarta...
T4 S500 B7 Y	Amostra 013 por Administrator data segun...
T6 S500 B7 Y	Amostra 016 por Administrator data quarta...
T8 S500 B7 Y	Amostra 028 por Administrator data terça-f...
T13 S500 B7 Y	Amostra 006 por Administrator data terça-f...
T18 S500 B7y	Amostra 011 por Administrator data quarta...
T24 S500 B7Y1	Amostra 011 por Administrator data segun...

Figura A.7. Espectros comparativos de FTIR-HATR da mistura B7 S500 (replicatas y) nos tempos 0, 2, 4, 6, 8, 13, 18 e 24 semanas de envelhecimento a 43 °C.

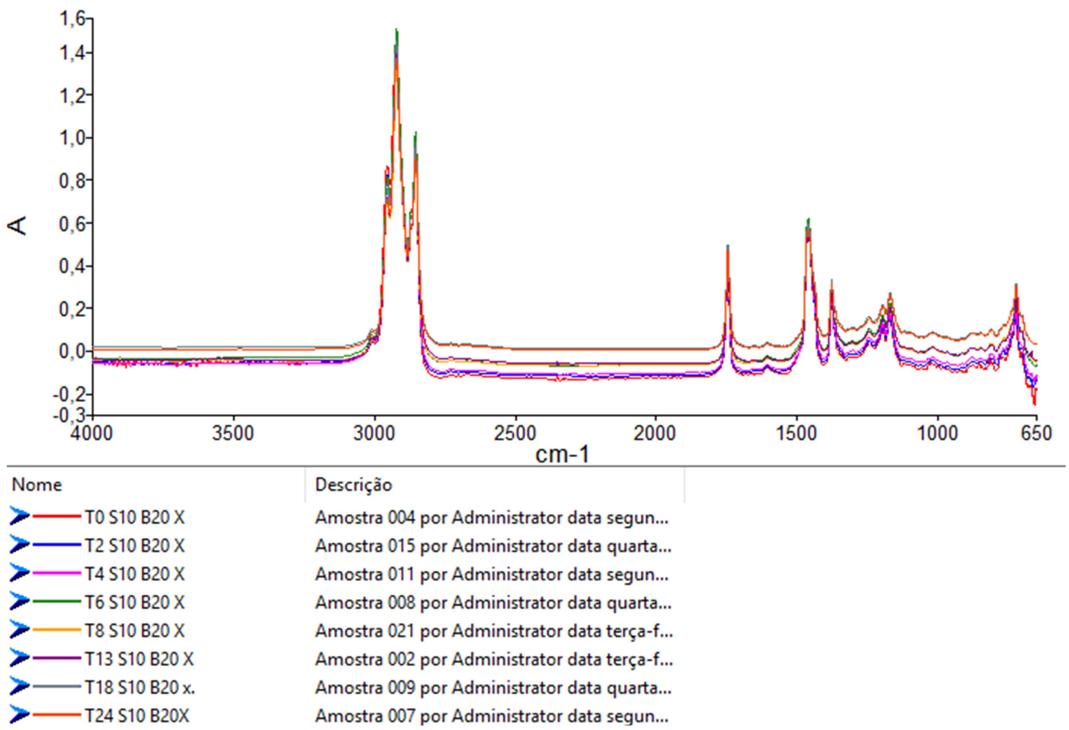

Nome	Descrição
T0 S10 B20 X	Amostra 004 por Administrator data segun...
T2 S10 B20 X	Amostra 015 por Administrator data quarta...
T4 S10 B20 X	Amostra 011 por Administrator data segun...
T6 S10 B20 X	Amostra 008 por Administrator data quarta...
T8 S10 B20 X	Amostra 021 por Administrator data terça-f...
T13 S10 B20 X	Amostra 002 por Administrator data terça-f...
T18 S10 B20 x.	Amostra 009 por Administrator data quarta...
T24 S10 B20X	Amostra 007 por Administrator data segun...

Figura A.8. Espectros comparativos de FTIR-HATR da mistura B20 S10 (replicatas x) nos tempos 0, 2, 4, 6, 8, 13, 18 e 24 semanas de envelhecimento a 43 °C.

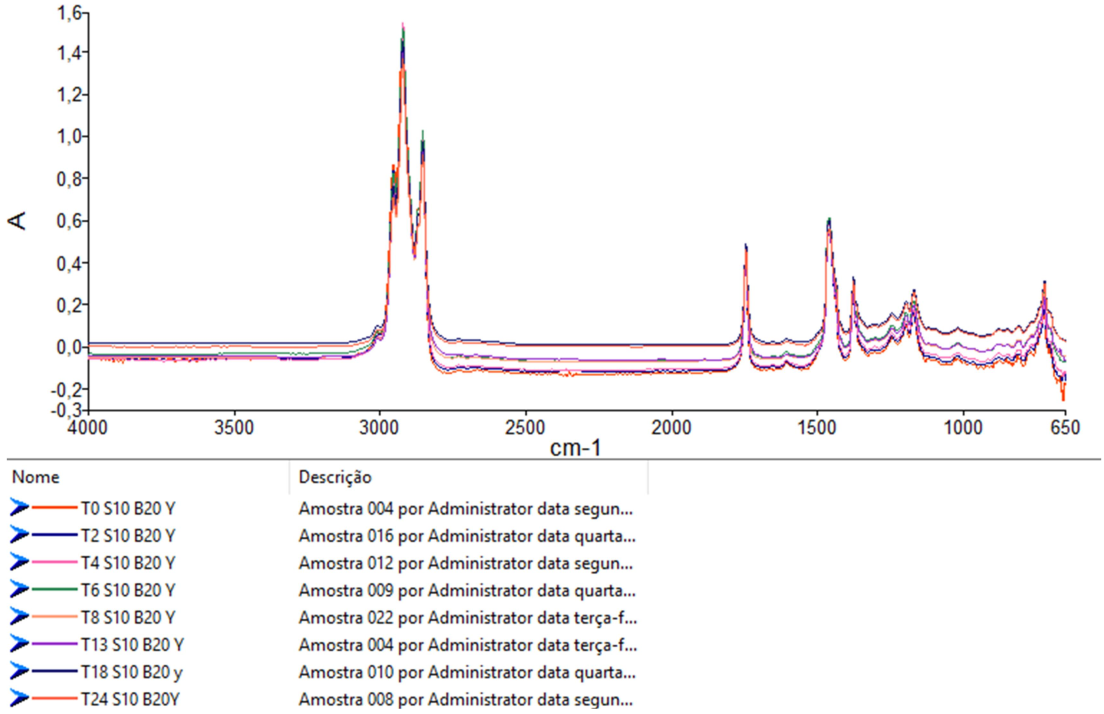

Nome	Descrição
T0 S10 B20 Y	Amostra 004 por Administrator data segun...
T2 S10 B20 Y	Amostra 016 por Administrator data quarta...
T4 S10 B20 Y	Amostra 012 por Administrator data segun...
T6 S10 B20 Y	Amostra 009 por Administrator data quarta...
T8 S10 B20 Y	Amostra 022 por Administrator data terça-f...
T13 S10 B20 Y	Amostra 004 por Administrator data terça-f...
T18 S10 B20 y	Amostra 010 por Administrator data quarta...
T24 S10 B20Y	Amostra 008 por Administrator data segun...

Figura A.9. Espectros comparativos de FTIR-HATR da mistura B20 S10 (replicatas y) nos tempos 0, 2, 4, 6, 8, 13, 18 e 24 semanas de envelhecimento a 43 °C.

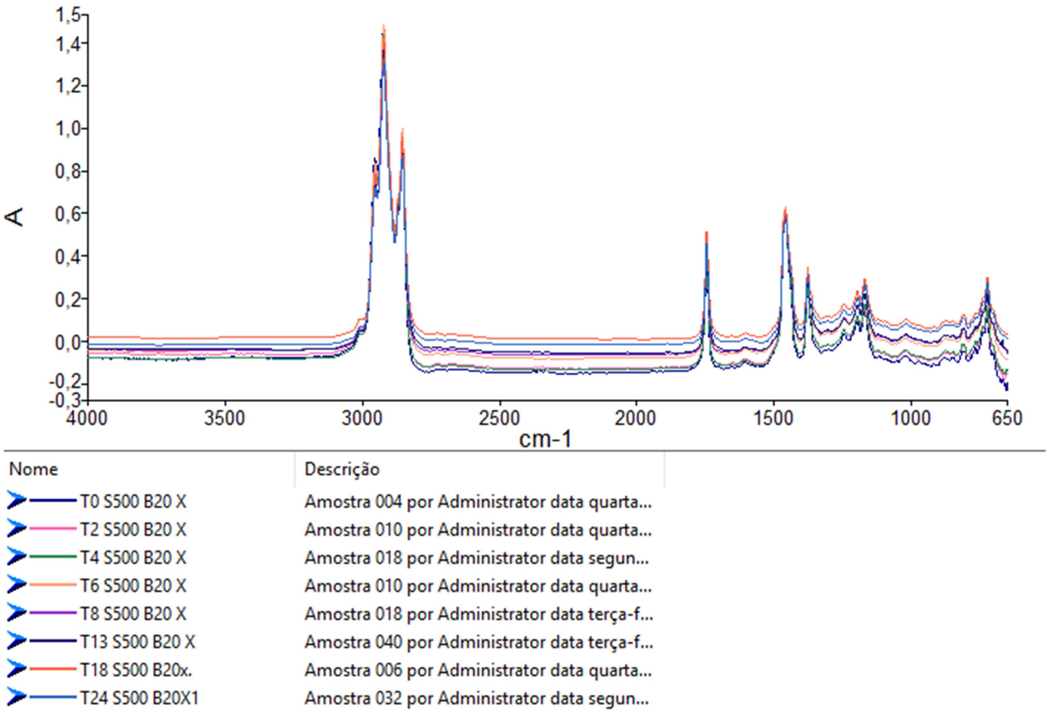

Nome	Descrição
T0 S500 B20 X	Amostra 004 por Administrator data quarta...
T2 S500 B20 X	Amostra 010 por Administrator data quarta...
T4 S500 B20 X	Amostra 018 por Administrator data segun...
T6 S500 B20 X	Amostra 010 por Administrator data quarta...
T8 S500 B20 X	Amostra 018 por Administrator data terça-f...
T13 S500 B20 X	Amostra 040 por Administrator data terça-f...
T18 S500 B20x.	Amostra 006 por Administrator data quarta...
T24 S500 B20X1	Amostra 032 por Administrator data segun...

Figura A.10. Espectros comparativos de FTIR-HATR da mistura B20 S500 (replicatas x) nos tempos 0, 2, 4, 6, 8, 13, 18 e 24 semanas de envelhecimento a 43 °C.

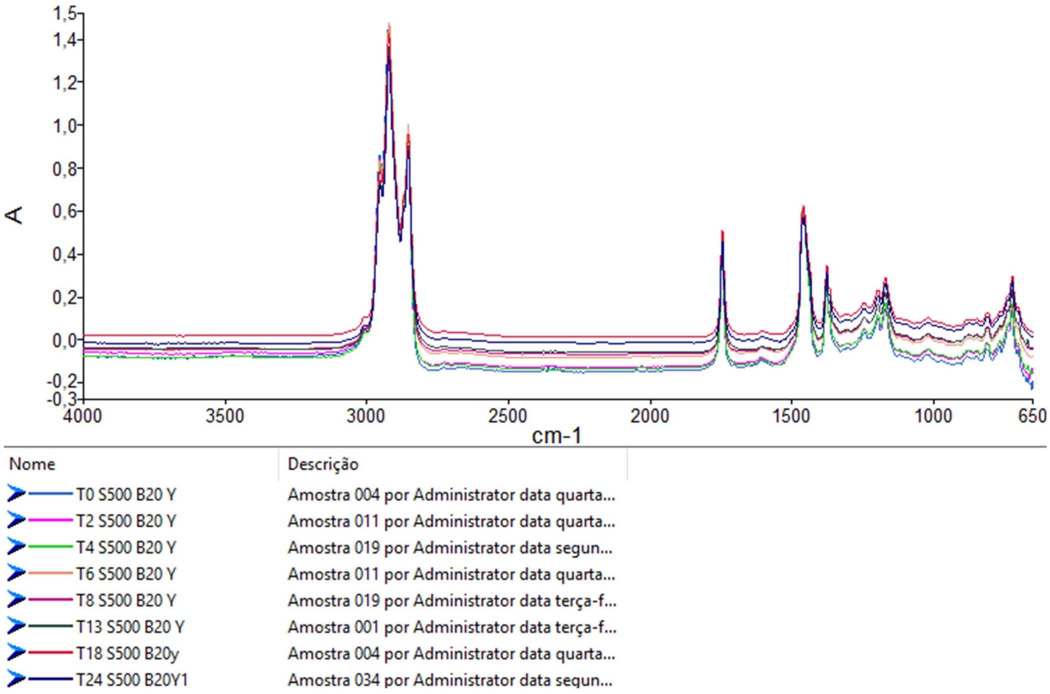

Nome	Descrição
T0 S500 B20 Y	Amostra 004 por Administrator data quarta...
T2 S500 B20 Y	Amostra 011 por Administrator data quarta...
T4 S500 B20 Y	Amostra 019 por Administrator data segun...
T6 S500 B20 Y	Amostra 011 por Administrator data quarta...
T8 S500 B20 Y	Amostra 019 por Administrator data terça-f...
T13 S500 B20 Y	Amostra 001 por Administrator data terça-f...
T18 S500 B20y	Amostra 004 por Administrator data quarta...
T24 S500 B20Y1	Amostra 034 por Administrator data segun...

Figura A.11. Espectros comparativos de FTIR-HATR da mistura B20 S500 (replicatas y) nos tempos 0, 2, 4, 6, 8, 13, 18 e 24 semanas de envelhecimento a 43 °C.

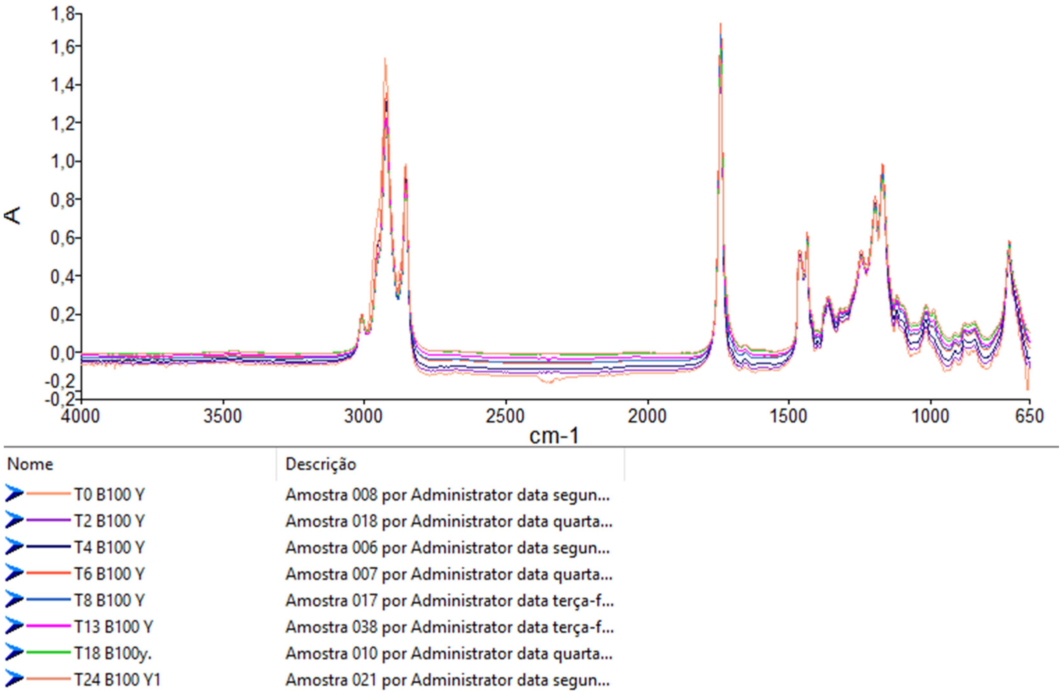

Nome	Descrição
T0 B100 Y	Amostra 008 por Administrator data segun...
T2 B100 Y	Amostra 018 por Administrator data quarta...
T4 B100 Y	Amostra 006 por Administrator data segun...
T6 B100 Y	Amostra 007 por Administrator data quarta...
T8 B100 Y	Amostra 017 por Administrator data terça-f...
T13 B100 Y	Amostra 038 por Administrator data terça-f...
T18 B100y.	Amostra 010 por Administrator data quarta...
T24 B100 Y1	Amostra 021 por Administrator data segun...

Figura A.12. Espectros comparativos de FTIR-HATR da mistura B100 (replicatas y) nos tempos 0, 2, 4, 6, 8, 13, 18 e 24 semanas de envelhecimento a 43 °C.

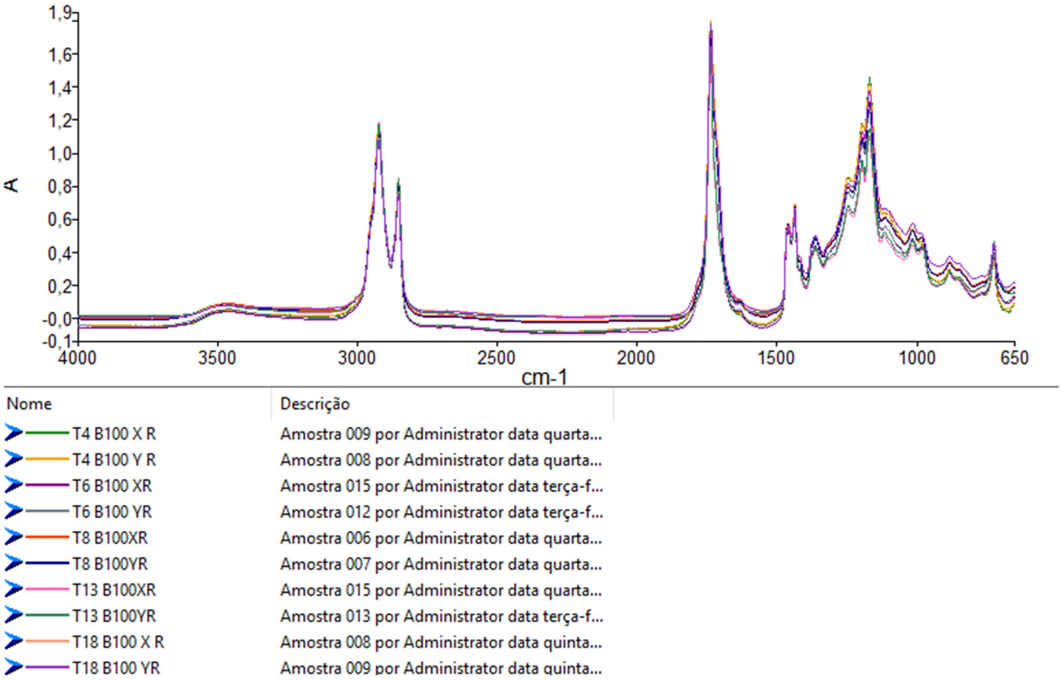

Nome	Descrição
T4 B100 X R	Amostra 009 por Administrator data quarta...
T4 B100 Y R	Amostra 008 por Administrator data quarta...
T6 B100 XR	Amostra 015 por Administrator data terça-f...
T6 B100 YR	Amostra 012 por Administrator data terça-f...
T8 B100XR	Amostra 006 por Administrator data quarta...
T8 B100YR	Amostra 007 por Administrator data quarta...
T13 B100XR	Amostra 015 por Administrator data quarta...
T13 B100YR	Amostra 013 por Administrator data terça-f...
T18 B100 X R	Amostra 008 por Administrator data quinta...
T18 B100 YR	Amostra 009 por Administrator data quinta...

Figura A.13. Espectros comparativos de FTIR-HATR dos resíduos da mistura B100 formados após o ensaio de Rancimat (replicatas x e y) nos tempos 4, 6, 8, 13 e 18 semanas de envelhecimento a 43 °C.

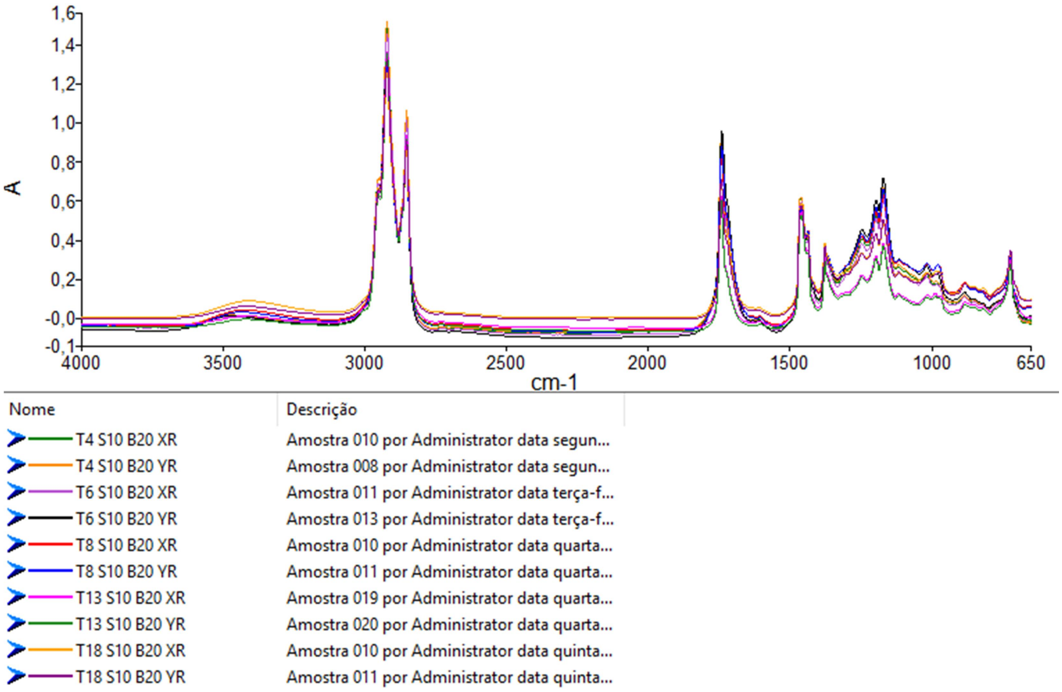

Nome	Descrição
T4 S10 B20 XR	Amostra 010 por Administrator data segun...
T4 S10 B20 YR	Amostra 008 por Administrator data segun...
T6 S10 B20 XR	Amostra 011 por Administrator data terça-f...
T6 S10 B20 YR	Amostra 013 por Administrator data terça-f...
T8 S10 B20 XR	Amostra 010 por Administrator data quarta...
T8 S10 B20 YR	Amostra 011 por Administrator data quarta...
T13 S10 B20 XR	Amostra 019 por Administrator data quarta...
T13 S10 B20 YR	Amostra 020 por Administrator data quarta...
T18 S10 B20 XR	Amostra 010 por Administrator data quinta...
T18 S10 B20 YR	Amostra 011 por Administrator data quinta...

Figura A.14. Espectros comparativos de FTIR-HATR dos resíduos da mistura B20 S10 formados após o ensaio de Rancimat® (replicatas x e y) nos tempos 4, 6, 8, 13 e 18 semanas de envelhecimento a 43 °C.

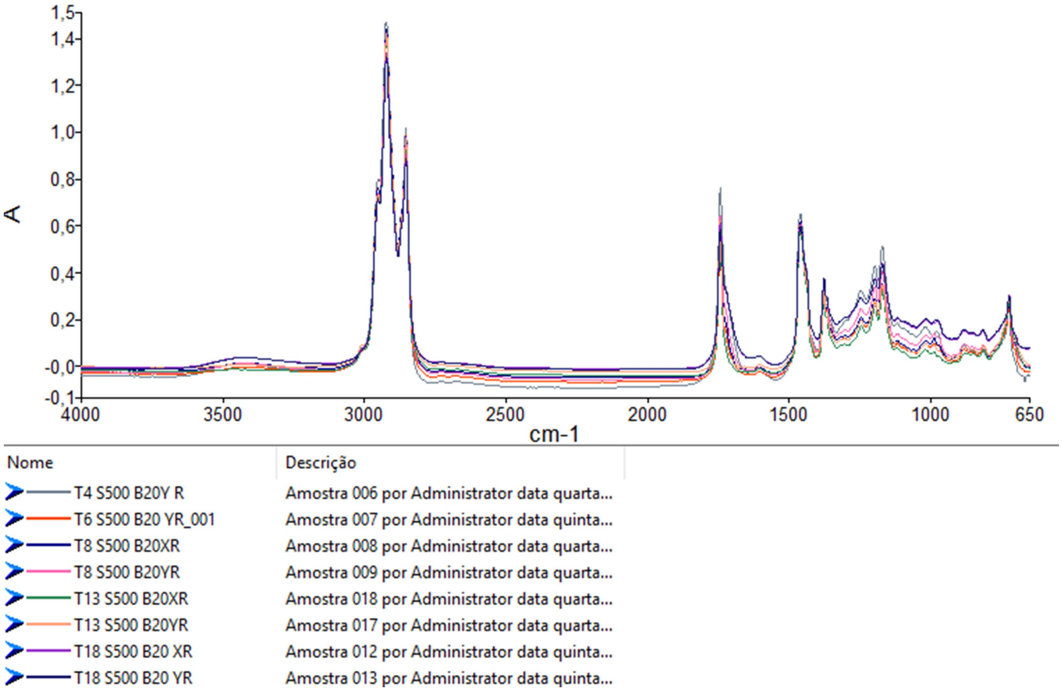

Nome	Descrição
T4 S500 B20Y R	Amostra 006 por Administrator data quarta...
T6 S500 B20 YR_001	Amostra 007 por Administrator data quinta...
T8 S500 B20XR	Amostra 008 por Administrator data quarta...
T8 S500 B20YR	Amostra 009 por Administrator data quarta...
T13 S500 B20XR	Amostra 018 por Administrator data quarta...
T13 S500 B20YR	Amostra 017 por Administrator data quarta...
T18 S500 B20 XR	Amostra 012 por Administrator data quinta...
T18 S500 B20 YR	Amostra 013 por Administrator data quinta...

Figura A.15. Espectros comparativos de FTIR-HATR dos resíduos da mistura B20 S500 formados após o ensaio de Rancimat® (replicatas x e y) nos tempos 4, 6, 8, 13 e 18 semanas de envelhecimento a 43 °C.

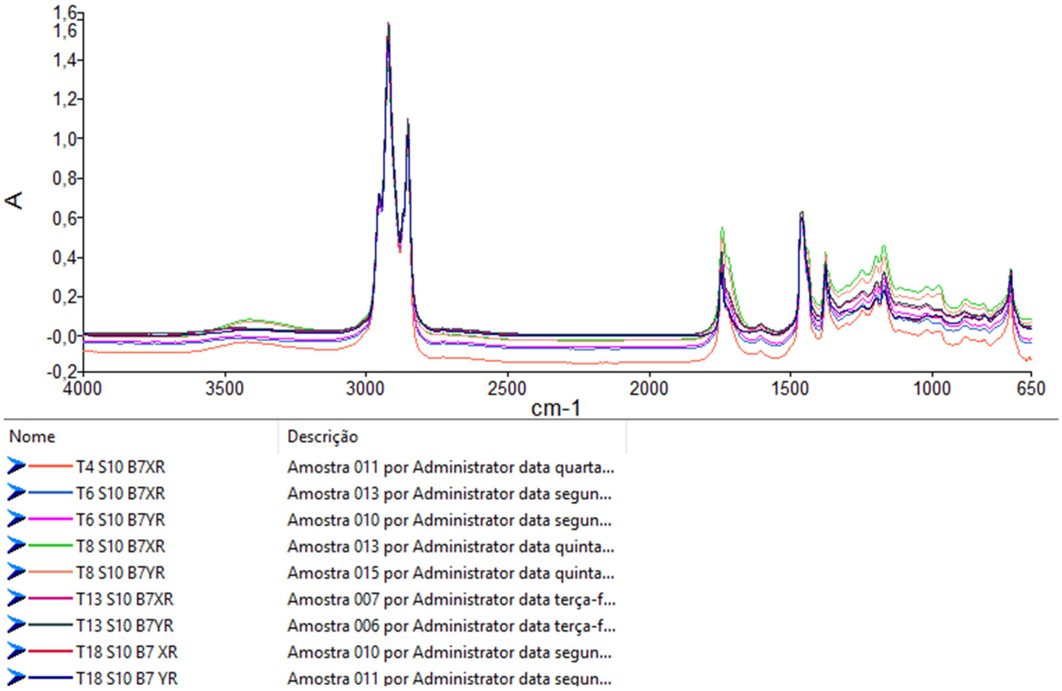

Nome	Descrição
T4 S10 B7XR	Amostra 011 por Administrator data quarta...
T6 S10 B7XR	Amostra 013 por Administrator data segun...
T6 S10 B7YR	Amostra 010 por Administrator data segun...
T8 S10 B7XR	Amostra 013 por Administrator data quinta...
T8 S10 B7YR	Amostra 015 por Administrator data quinta...
T13 S10 B7XR	Amostra 007 por Administrator data terça-f...
T13 S10 B7YR	Amostra 006 por Administrator data terça-f...
T18 S10 B7 XR	Amostra 010 por Administrator data segun...
T18 S10 B7 YR	Amostra 011 por Administrator data segun...

Figura A.16. Espectros comparativos de FTIR-HATR dos resíduos da mistura B7 S10 formados após o ensaio de Rancimat® (replicatas x e y) nos tempos 4, 6, 8, 13 e 18 semanas de envelhecimento a 43 °C.

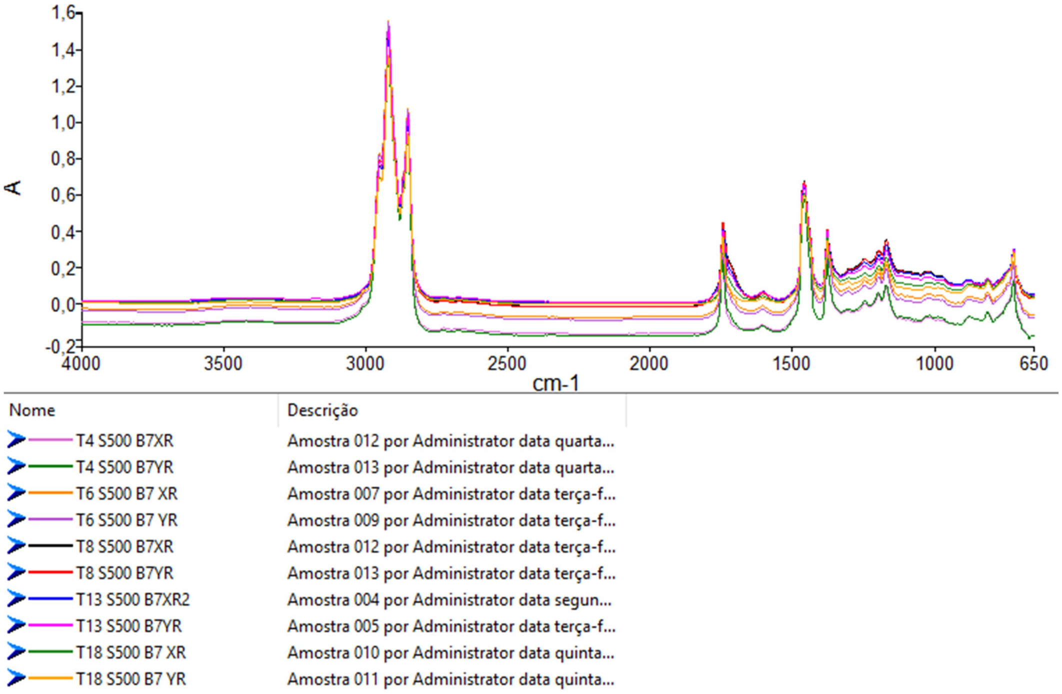

Nome	Descrição
T4 S500 B7XR	Amostra 012 por Administrator data quarta...
T4 S500 B7YR	Amostra 013 por Administrator data quarta...
T6 S500 B7 XR	Amostra 007 por Administrator data terça-f...
T6 S500 B7 YR	Amostra 009 por Administrator data terça-f...
T8 S500 B7XR	Amostra 012 por Administrator data terça-f...
T8 S500 B7YR	Amostra 013 por Administrator data terça-f...
T13 S500 B7XR2	Amostra 004 por Administrator data segun...
T13 S500 B7YR	Amostra 005 por Administrator data terça-f...
T18 S500 B7 XR	Amostra 010 por Administrator data quinta...
T18 S500 B7 YR	Amostra 011 por Administrator data quinta...

Figura A.17. Espectros comparativos de FTIR-HATR dos resíduos da mistura B7 S500 formados após o ensaio de Rancimat® (replicatas x e y) nos tempos 4, 6, 8, 13 e 18 semanas de envelhecimento a 43 °C.

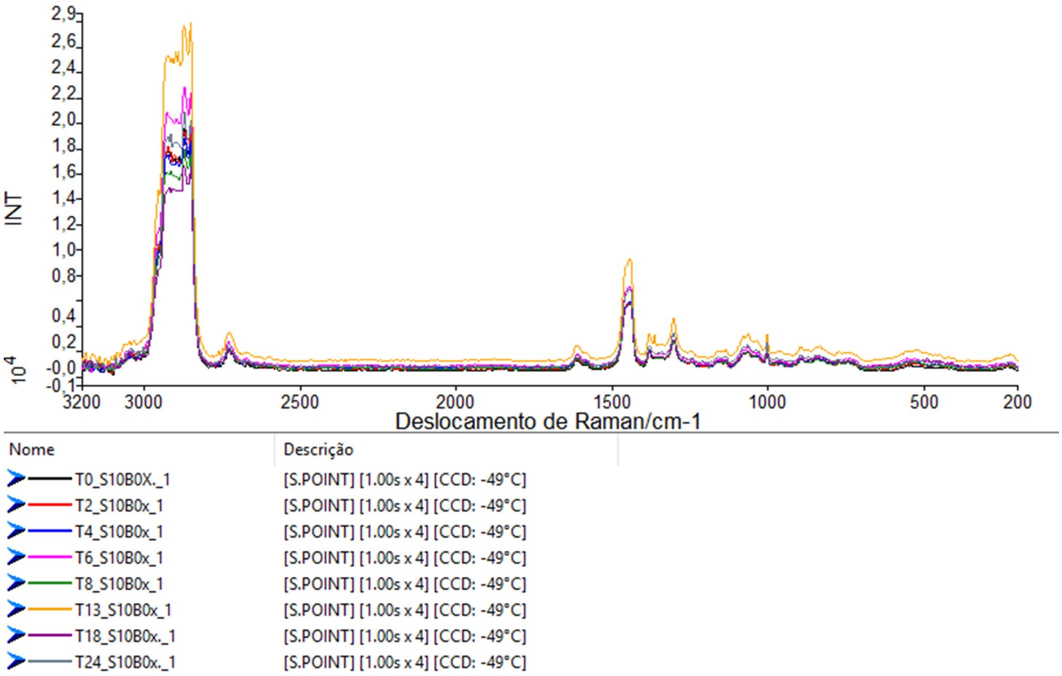

Nome	Descrição
T0_S10B0X._1	[S.POINT] [1.00s x 4] [CCD: -49°C]
T2_S10B0x_1	[S.POINT] [1.00s x 4] [CCD: -49°C]
T4_S10B0x_1	[S.POINT] [1.00s x 4] [CCD: -49°C]
T6_S10B0x_1	[S.POINT] [1.00s x 4] [CCD: -49°C]
T8_S10B0x_1	[S.POINT] [1.00s x 4] [CCD: -49°C]
T13_S10B0x_1	[S.POINT] [1.00s x 4] [CCD: -49°C]
T18_S10B0x._1	[S.POINT] [1.00s x 4] [CCD: -49°C]
T24_S10B0x._1	[S.POINT] [1.00s x 4] [CCD: -49°C]

Figura A.18. Espectros comparativos de Raman da mistura B0 S10 (replicatas x) nos tempos 0, 2, 4, 6, 8, 13, 18 e 24 semanas de envelhecimento a 43 °C.

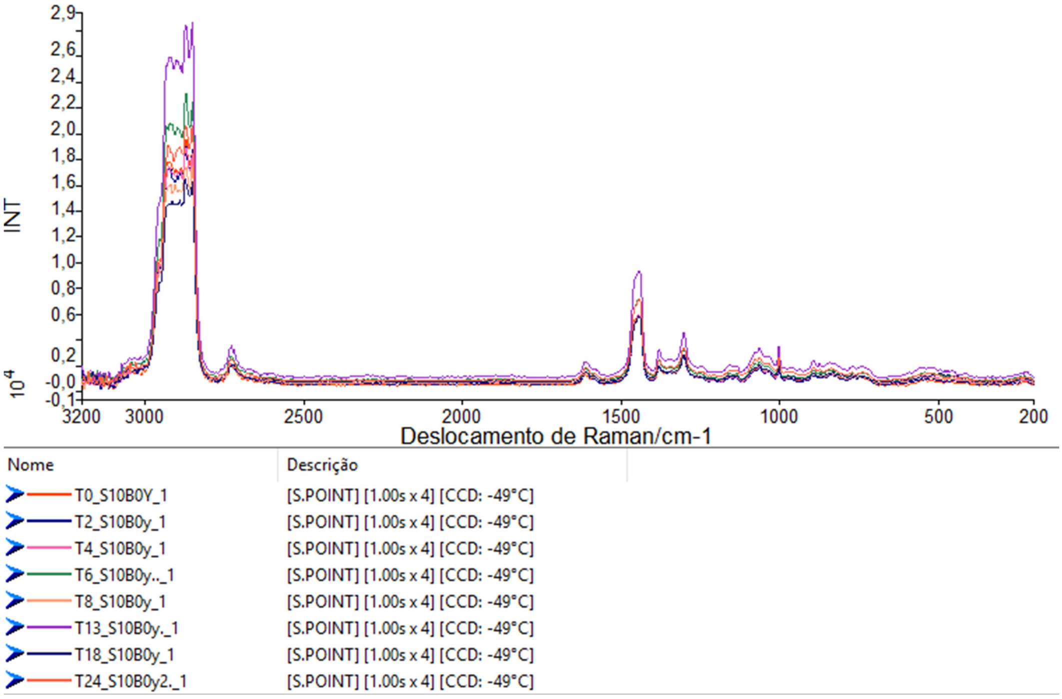

Nome	Descrição
T0_S10B0Y_1	[S.POINT] [1.00s x 4] [CCD: -49°C]
T2_S10B0y_1	[S.POINT] [1.00s x 4] [CCD: -49°C]
T4_S10B0y_1	[S.POINT] [1.00s x 4] [CCD: -49°C]
T6_S10B0y.._1	[S.POINT] [1.00s x 4] [CCD: -49°C]
T8_S10B0y_1	[S.POINT] [1.00s x 4] [CCD: -49°C]
T13_S10B0y._1	[S.POINT] [1.00s x 4] [CCD: -49°C]
T18_S10B0y_1	[S.POINT] [1.00s x 4] [CCD: -49°C]
T24_S10B0y2._1	[S.POINT] [1.00s x 4] [CCD: -49°C]

Figura A.19. Espectros comparativos de Raman da mistura B0 S10 (replicatas y) nos tempos 0, 2, 4, 6, 8, 13, 18 e 24 semanas de envelhecimento a 43 °C.

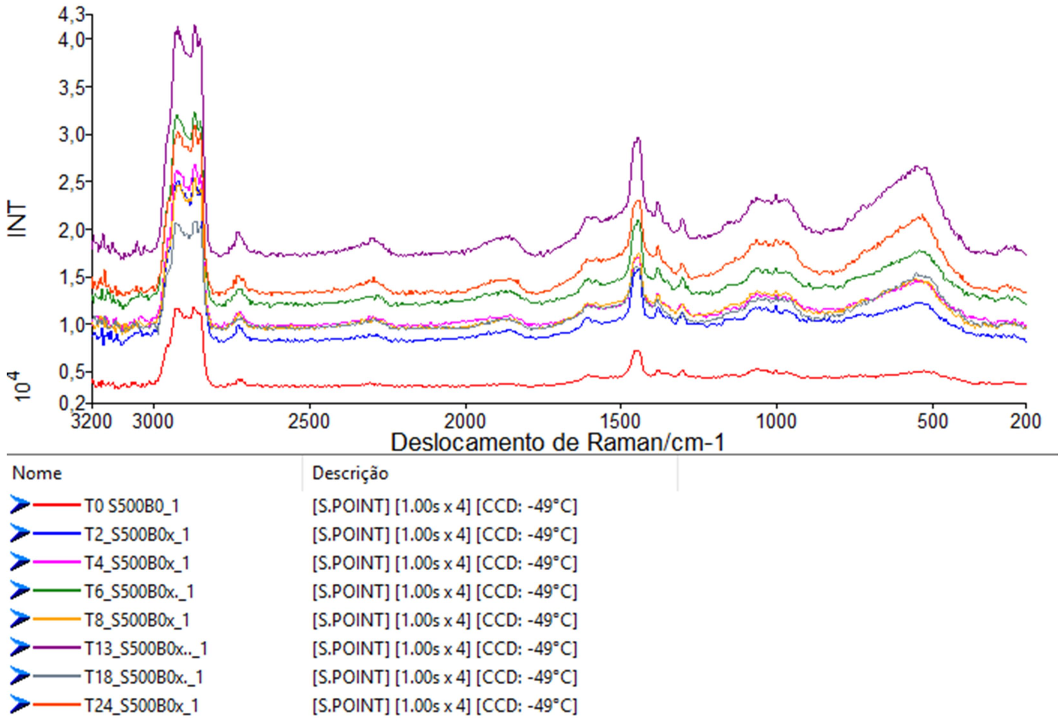

Nome	Descrição
T0 S500B0_1	[S.POINT] [1.00s x 4] [CCD: -49°C]
T2_S500B0x_1	[S.POINT] [1.00s x 4] [CCD: -49°C]
T4_S500B0x_1	[S.POINT] [1.00s x 4] [CCD: -49°C]
T6_S500B0x._1	[S.POINT] [1.00s x 4] [CCD: -49°C]
T8_S500B0x_1	[S.POINT] [1.00s x 4] [CCD: -49°C]
T13_S500B0x.._1	[S.POINT] [1.00s x 4] [CCD: -49°C]
T18_S500B0x._1	[S.POINT] [1.00s x 4] [CCD: -49°C]
T24_S500B0x_1	[S.POINT] [1.00s x 4] [CCD: -49°C]

Figura A.20. Espectros comparativos de Raman da mistura B0 S500 (replicatas x) nos tempos 0, 2, 4, 6, 8, 13, 18 e 24 semanas de envelhecimento a 43 °C.

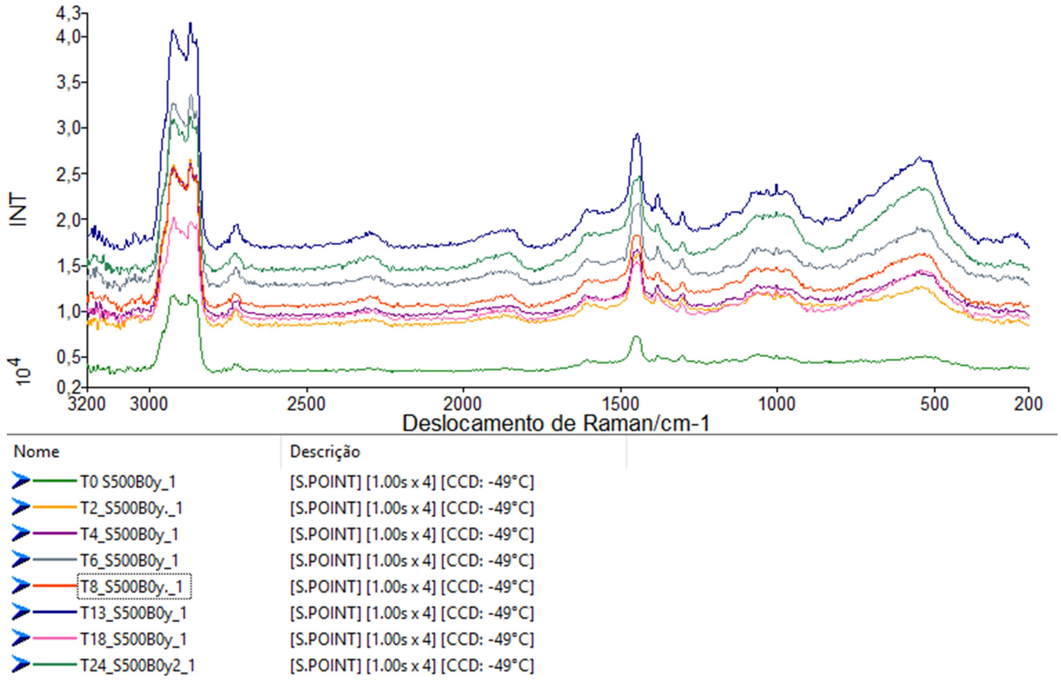

Nome	Descrição
T0 S500B0y_1	[S.POINT] [1.00s x 4] [CCD: -49°C]
T2_S500B0y._1	[S.POINT] [1.00s x 4] [CCD: -49°C]
T4_S500B0y_1	[S.POINT] [1.00s x 4] [CCD: -49°C]
T6_S500B0y_1	[S.POINT] [1.00s x 4] [CCD: -49°C]
T8_S500B0y._1	[S.POINT] [1.00s x 4] [CCD: -49°C]
T13_S500B0y_1	[S.POINT] [1.00s x 4] [CCD: -49°C]
T18_S500B0y_1	[S.POINT] [1.00s x 4] [CCD: -49°C]
T24_S500B0y2_1	[S.POINT] [1.00s x 4] [CCD: -49°C]

Figura A.21. Espectros comparativos de Raman da mistura B0 S500 (replicatas y) nos tempos 0, 2, 4, 6, 8, 13, 18 e 24 semanas de envelhecimento a 43 °C.

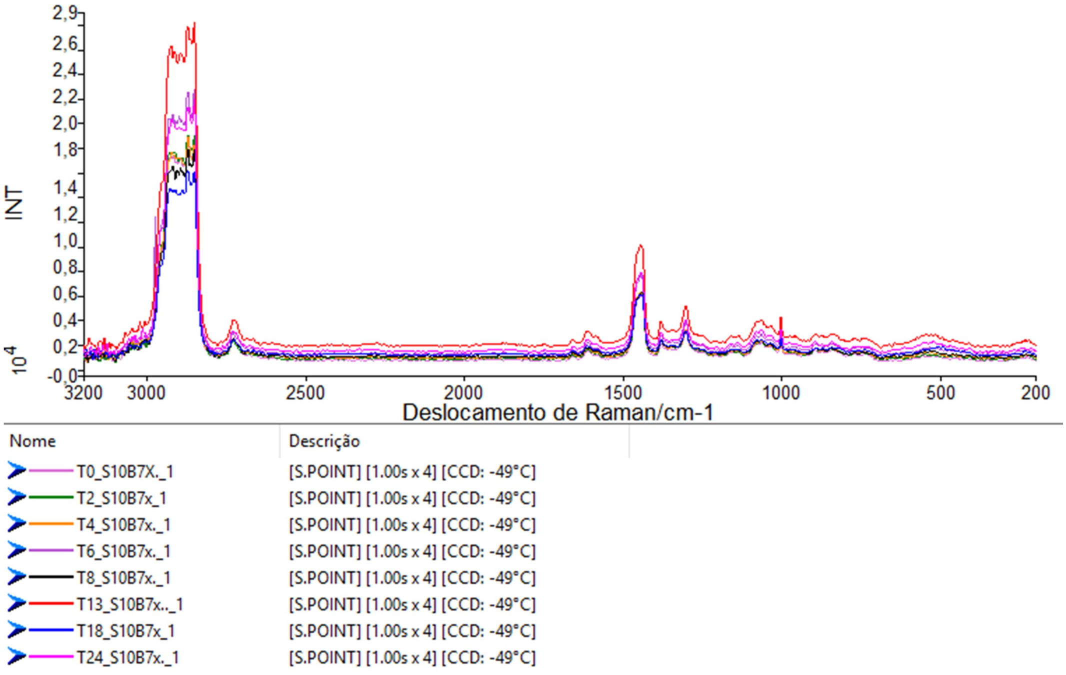

Nome	Descrição
T0_S10B7X._1	[S.POINT] [1.00s x 4] [CCD: -49°C]
T2_S10B7x_1	[S.POINT] [1.00s x 4] [CCD: -49°C]
T4_S10B7x._1	[S.POINT] [1.00s x 4] [CCD: -49°C]
T6_S10B7x._1	[S.POINT] [1.00s x 4] [CCD: -49°C]
T8_S10B7x._1	[S.POINT] [1.00s x 4] [CCD: -49°C]
T13_S10B7x.._1	[S.POINT] [1.00s x 4] [CCD: -49°C]
T18_S10B7x_1	[S.POINT] [1.00s x 4] [CCD: -49°C]
T24_S10B7x._1	[S.POINT] [1.00s x 4] [CCD: -49°C]

Figura A.22. Espectros comparativos de Raman da mistura B7 S10 (replicatas x) nos tempos 0, 2, 4, 6, 8, 13, 18 e 24 semanas de envelhecimento a 43 °C.

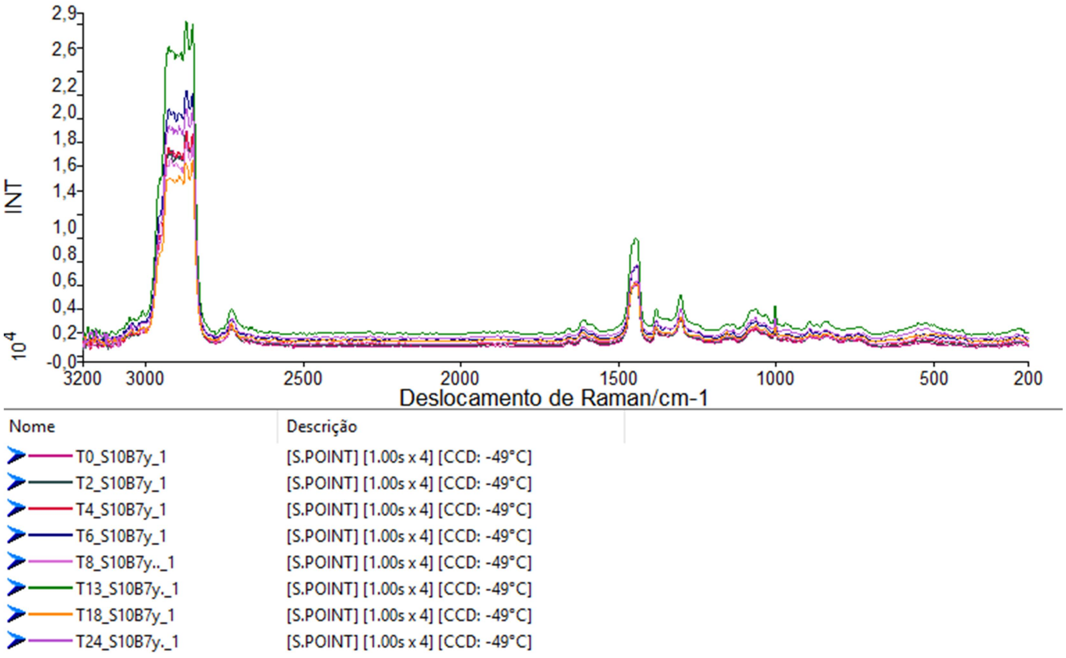

Nome	Descrição
T0_S10B7y_1	[S.POINT] [1.00s x 4] [CCD: -49°C]
T2_S10B7y_1	[S.POINT] [1.00s x 4] [CCD: -49°C]
T4_S10B7y_1	[S.POINT] [1.00s x 4] [CCD: -49°C]
T6_S10B7y_1	[S.POINT] [1.00s x 4] [CCD: -49°C]
T8_S10B7y.._1	[S.POINT] [1.00s x 4] [CCD: -49°C]
T13_S10B7y._1	[S.POINT] [1.00s x 4] [CCD: -49°C]
T18_S10B7y_1	[S.POINT] [1.00s x 4] [CCD: -49°C]
T24_S10B7y._1	[S.POINT] [1.00s x 4] [CCD: -49°C]

Figura A.23. Espectros comparativos de Raman da mistura B7 S10 (replicatas y) nos tempos 0, 2, 4, 6, 8, 13, 18 e 24 semanas de envelhecimento a 43 °C.

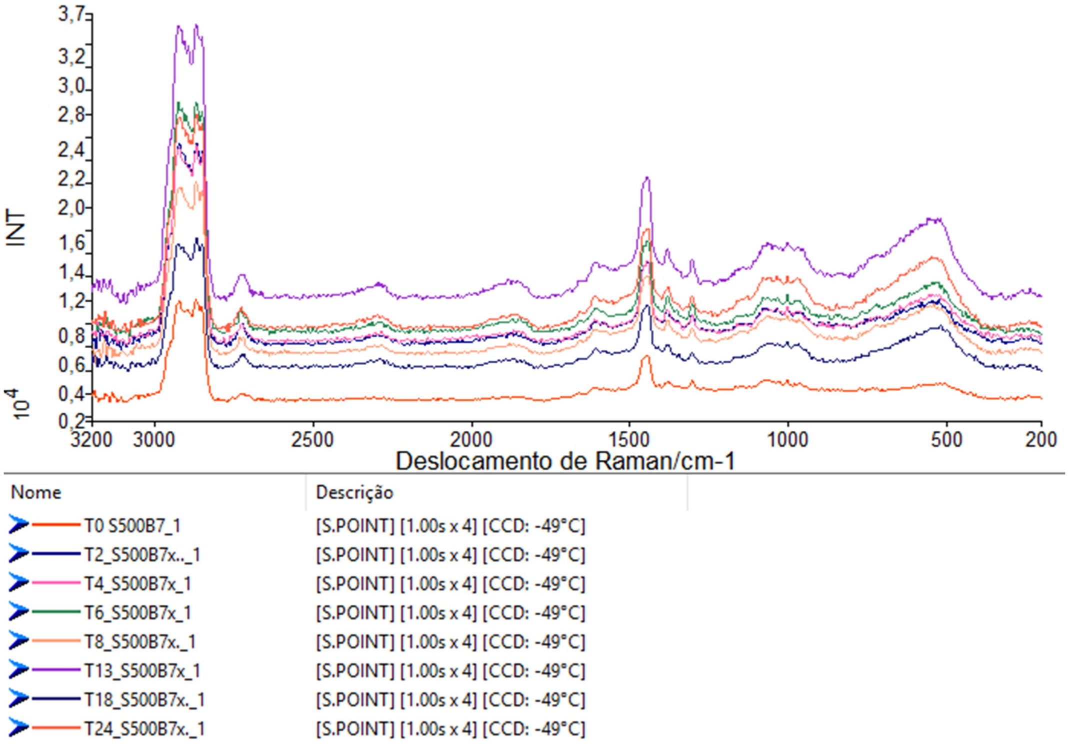

Nome	Descrição
T0 S500B7_1	[S.POINT] [1.00s x 4] [CCD: -49°C]
T2_S500B7x.._1	[S.POINT] [1.00s x 4] [CCD: -49°C]
T4_S500B7x_1	[S.POINT] [1.00s x 4] [CCD: -49°C]
T6_S500B7x_1	[S.POINT] [1.00s x 4] [CCD: -49°C]
T8_S500B7x._1	[S.POINT] [1.00s x 4] [CCD: -49°C]
T13_S500B7x_1	[S.POINT] [1.00s x 4] [CCD: -49°C]
T18_S500B7x._1	[S.POINT] [1.00s x 4] [CCD: -49°C]
T24_S500B7x._1	[S.POINT] [1.00s x 4] [CCD: -49°C]

Figura A.24. Espectros comparativos de Raman da mistura B7 S500 (replicatas x) nos tempos 0, 2, 4, 6, 8, 13, 18 e 24 semanas de envelhecimento a 43 °C.

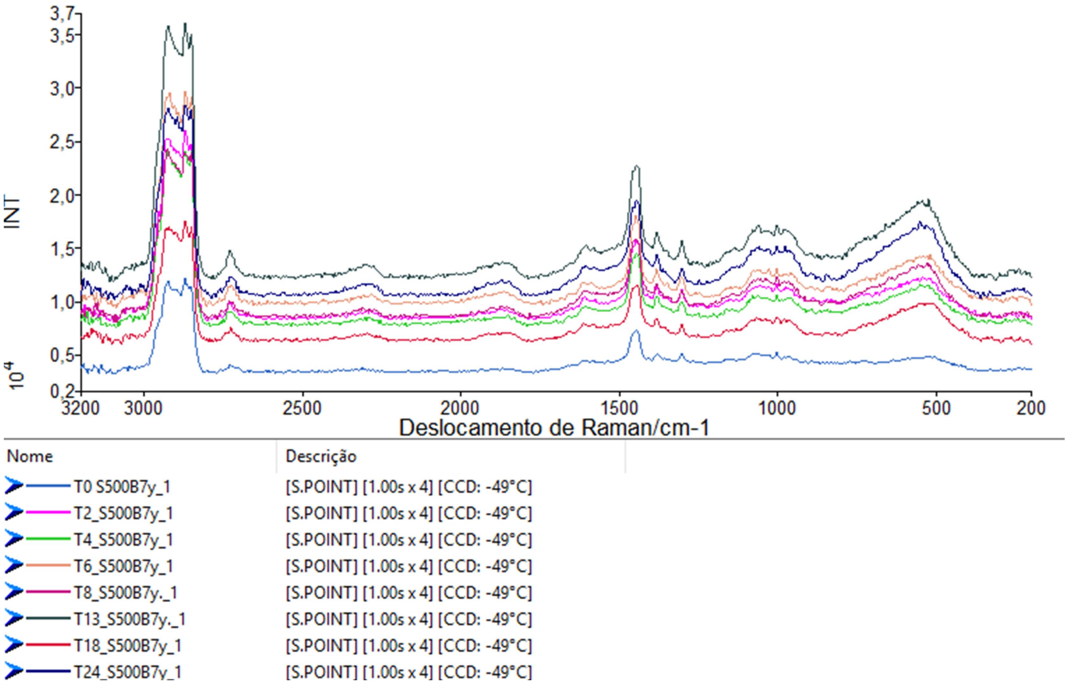

Nome	Descrição
T0 S500B7y_1	[S.POINT] [1.00s x 4] [CCD: -49°C]
T2_S500B7y_1	[S.POINT] [1.00s x 4] [CCD: -49°C]
T4_S500B7y_1	[S.POINT] [1.00s x 4] [CCD: -49°C]
T6_S500B7y_1	[S.POINT] [1.00s x 4] [CCD: -49°C]
T8_S500B7y._1	[S.POINT] [1.00s x 4] [CCD: -49°C]
T13_S500B7y._1	[S.POINT] [1.00s x 4] [CCD: -49°C]
T18_S500B7y_1	[S.POINT] [1.00s x 4] [CCD: -49°C]
T24_S500B7y_1	[S.POINT] [1.00s x 4] [CCD: -49°C]

Figura A.25. Espectros comparativos de Raman da mistura B7 S500 (replicatas y) nos tempos 0, 2, 4, 6, 8, 13, 18 e 24 semanas de envelhecimento a 43 °C.

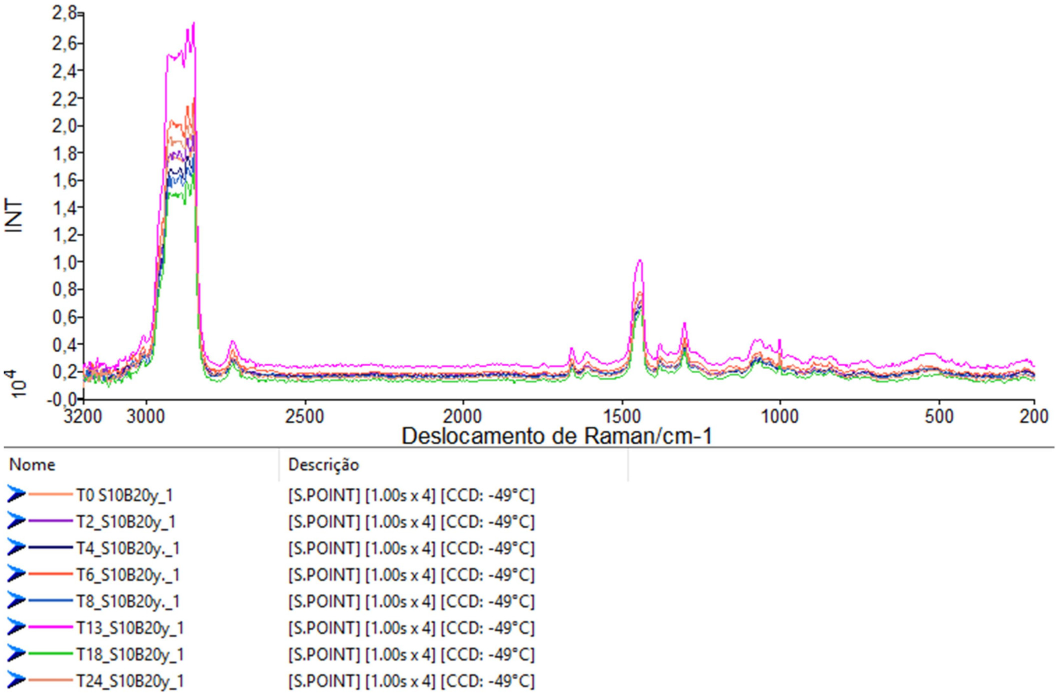

Nome	Descrição
T0 S10B20y_1	[S.POINT] [1.00s x 4] [CCD: -49°C]
T2_S10B20y_1	[S.POINT] [1.00s x 4] [CCD: -49°C]
T4_S10B20y._1	[S.POINT] [1.00s x 4] [CCD: -49°C]
T6_S10B20y._1	[S.POINT] [1.00s x 4] [CCD: -49°C]
T8_S10B20y._1	[S.POINT] [1.00s x 4] [CCD: -49°C]
T13_S10B20y_1	[S.POINT] [1.00s x 4] [CCD: -49°C]
T18_S10B20y_1	[S.POINT] [1.00s x 4] [CCD: -49°C]
T24_S10B20y_1	[S.POINT] [1.00s x 4] [CCD: -49°C]

Figura A.26 Espectros comparativos de Raman da mistura B20 S10 (replicatas y) nos tempos 0, 2, 4, 6, 8, 13, 18 e 24 semanas de envelhecimento a 43 °C.

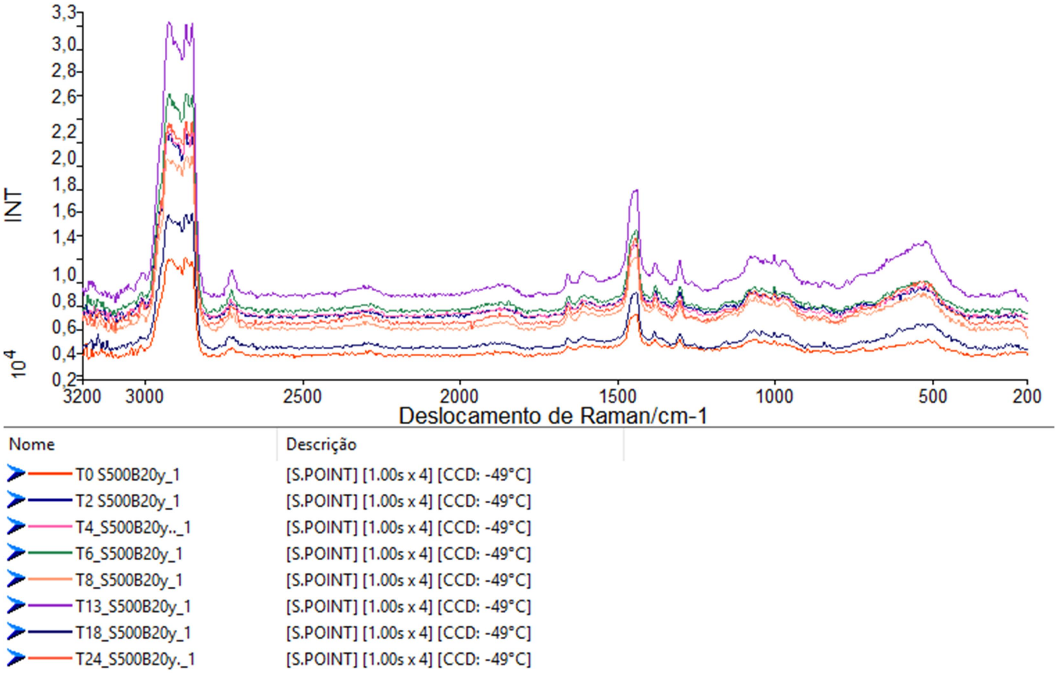

Nome	Descrição
T0 S500B20y_1	[S.POINT] [1.00s x 4] [CCD: -49°C]
T2 S500B20y_1	[S.POINT] [1.00s x 4] [CCD: -49°C]
T4_S500B20y.._1	[S.POINT] [1.00s x 4] [CCD: -49°C]
T6_S500B20y_1	[S.POINT] [1.00s x 4] [CCD: -49°C]
T8_S500B20y_1	[S.POINT] [1.00s x 4] [CCD: -49°C]
T13_S500B20y_1	[S.POINT] [1.00s x 4] [CCD: -49°C]
T18_S500B20y_1	[S.POINT] [1.00s x 4] [CCD: -49°C]
T24_S500B20y._1	[S.POINT] [1.00s x 4] [CCD: -49°C]

Figura A.27. Espectros comparativos de Raman da mistura B20 S500 (replicatas y) nos tempos 0, 2, 4, 6, 8, 13, 18 e 24 semanas de envelhecimento a 43 °C.

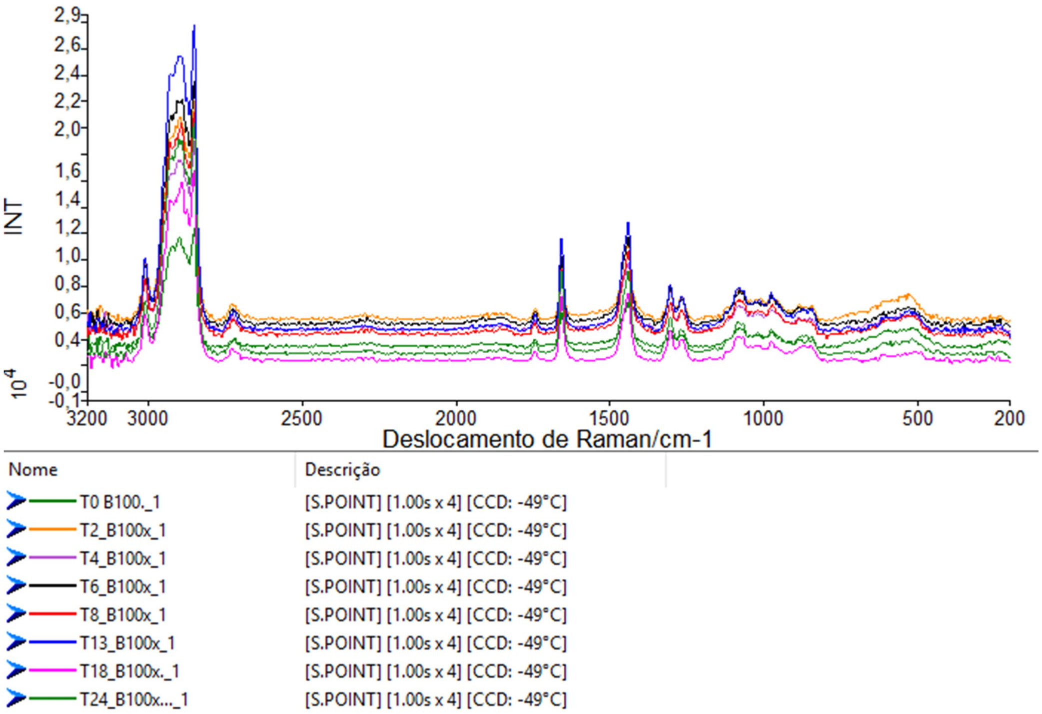

Nome	Descrição
T0 B100._1	[S.POINT] [1.00s x 4] [CCD: -49°C]
T2_B100x_1	[S.POINT] [1.00s x 4] [CCD: -49°C]
T4_B100x_1	[S.POINT] [1.00s x 4] [CCD: -49°C]
T6_B100x_1	[S.POINT] [1.00s x 4] [CCD: -49°C]
T8_B100x_1	[S.POINT] [1.00s x 4] [CCD: -49°C]
T13_B100x_1	[S.POINT] [1.00s x 4] [CCD: -49°C]
T18_B100x._1	[S.POINT] [1.00s x 4] [CCD: -49°C]
T24_B100x..._1	[S.POINT] [1.00s x 4] [CCD: -49°C]

Figura A.28. Espectros comparativos de Raman da mistura B100 (replicatas x) nos tempos 0, 2, 4, 6, 8, 13, 18 e 24 semanas de envelhecimento a 43 °C.

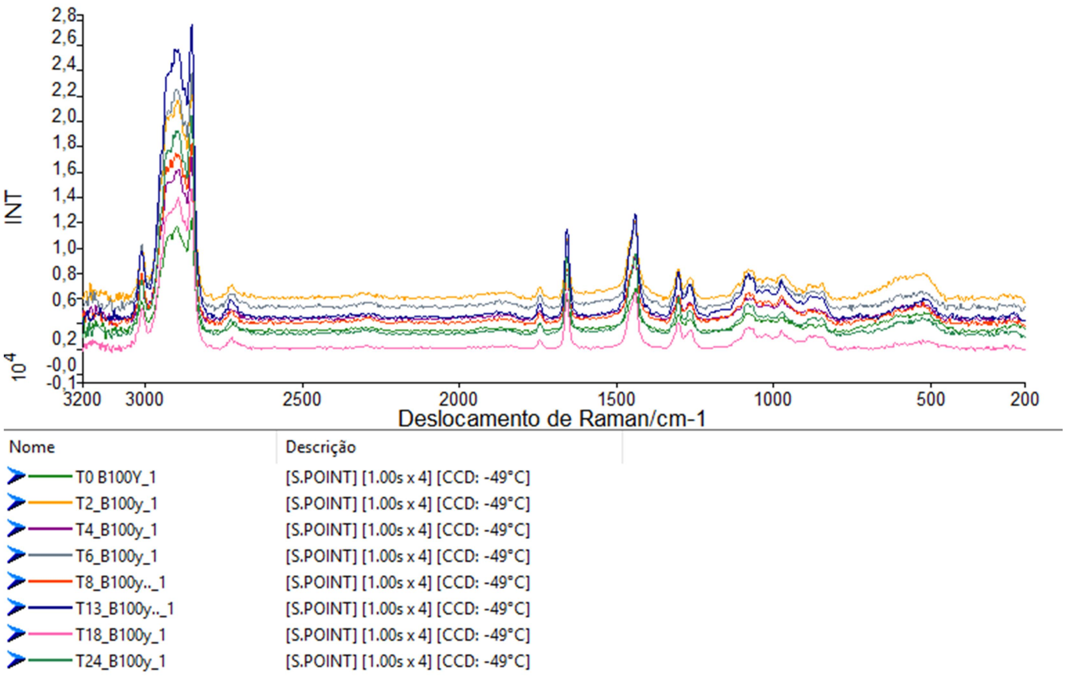

Nome	Descrição
T0 B100Y_1	[S.POINT] [1.00s x 4] [CCD: -49°C]
T2_B100y_1	[S.POINT] [1.00s x 4] [CCD: -49°C]
T4_B100y_1	[S.POINT] [1.00s x 4] [CCD: -49°C]
T6_B100y_1	[S.POINT] [1.00s x 4] [CCD: -49°C]
T8_B100y.._1	[S.POINT] [1.00s x 4] [CCD: -49°C]
T13_B100y.._1	[S.POINT] [1.00s x 4] [CCD: -49°C]
T18_B100y_1	[S.POINT] [1.00s x 4] [CCD: -49°C]
T24_B100y_1	[S.POINT] [1.00s x 4] [CCD: -49°C]

Figura A.29. Espectros comparativos de Raman da mistura B100 (replicatas y) nos tempos 0, 2, 4, 6, 8, 13, 18 e 24 semanas de envelhecimento a 43 °C.

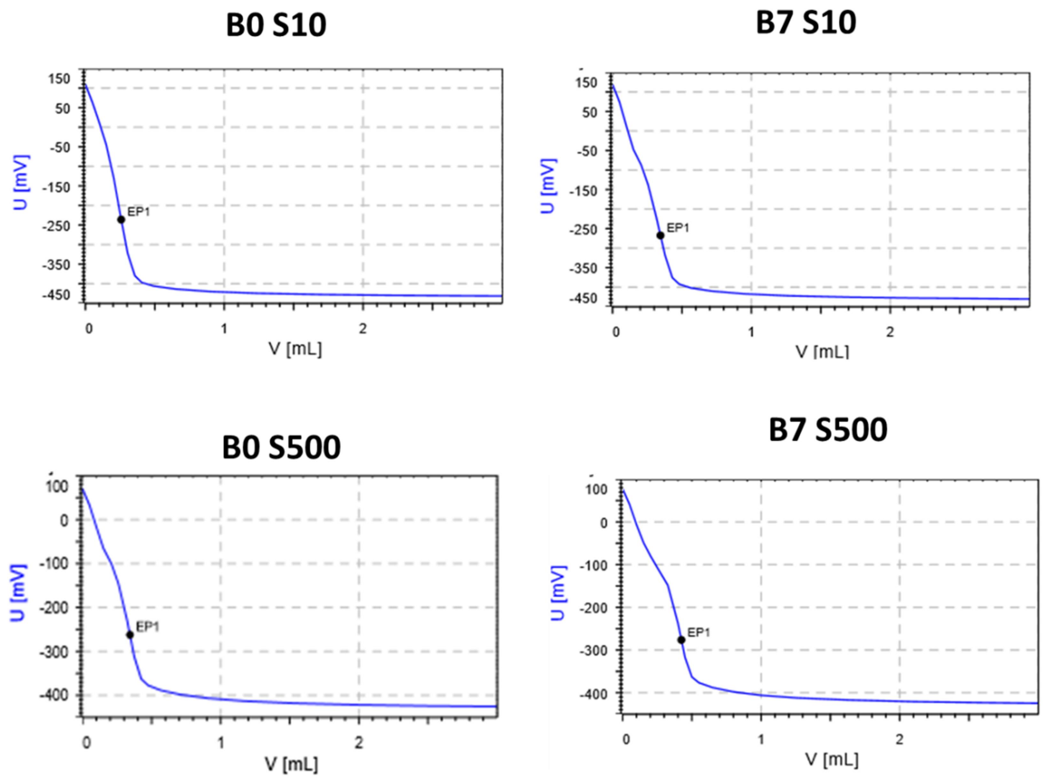

Figura A.30. Perfis das curvas de titulação do índice de acidez das misturas B0 S10, B0 S500, B7 S10 e B7 S500 no tempo inicial do experimento (t_0).

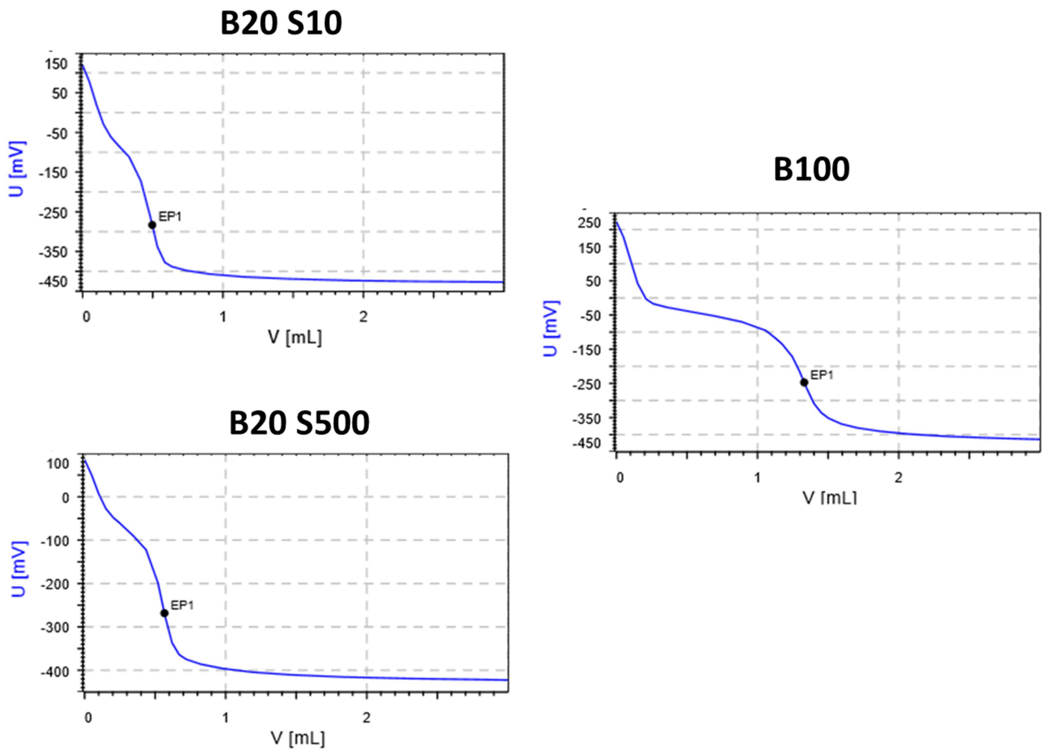

Figura A.31. Perfis das curvas de titulação do índice de acidez das misturas B20 S10, B20 S500 e B100 no tempo inicial do experimento (t_0).

9. Apêndice

Artigo publicado na revista da *American Chemical Society* "*Energy & Fuels*", de alto fator de impacto (2,835).

energy&fuels
Article
pubs.acs.org/EF

Physicochemical Characterization of Commercial Biodiesel/Diesel Blends and Evaluation of Unconventional Spectroscopic Vibrational Techniques in the Monitoring of Their Oxidation and Hydrolysis during Storage

Vanessa Souza Breder Valente,[†,‡] Andréa dos Santos Vieira,[†] Roberta Miranda Teixeira,[‡] and Nicolás A. Rey*[,†]

[†]Department of Chemistry, Pontifical Catholic University of Rio de Janeiro (PUC-Rio), Rua Marquês de São Vicente, 225 Gávea, Rio de Janeiro/RJ, 22.451-900 Brazil

[‡]Ipiranga Produtos de Petróleo S.A., Rua Monsenhor Manuel Gomes, 140 São Cristovão, Rio de Janeiro/RJ, 20.931-670 Brazil

ABSTRACT: A series of physicochemical studies performed on Brazilian commercial Bx (0%, 7%, 20%, and 100% soybean/tallow biodiesel) mixtures in S10 and S500 oil diesel, as well as the performance of two rapid and still underexplored techniques, namely, FTIR-HATR and Raman spectroscopies, to evaluate the hydrolysis and oxidative stability of these blends are reported. The addition of biodiesel to diesel affects negatively the aging resistance of the resulting blends. S500 blends are more acidic than S10 blends, in accordance with the higher water content of the former. Rancimat accelerated oxidative stability tests showed that, as expected, the induction times of B7 and B20 samples are greater than that of B100, independent of the sulfur content of the diesel. The practical use of FTIR-HATR to characterize the mixtures' degradation stage is conditioned by the fact that there are two chemical contributions for the studied band. On the other hand, Raman spectroscopy represents a very suitable spectroscopic probe for unsaturations in the fatty acids chains of biodiesel. Since FTIR-HATR and Raman spectroscopies do not require any sample preparation, are fast and quite low cost techniques, and cause low impact to the environment, further attention must be paid to their use in the analysis of biodiesel-containing fuels degradation.

1. INTRODUCTION

The global energy crisis, as well as environmental preservation, have directed the companies to look at the renewable energy sources. Among these is biodiesel, which is usually obtained by the catalytic transesterification reaction between a vegetable oil or an animal fat and short chain alcohols. Biodiesel comprises a blend of fatty acid esters having similar properties to those of fossil fuel, making it possible to use it as a substituent for petroleum diesel, or even to employ biodiesel/diesel mixtures.[1]

Although Brazil has a diversity of vegetable oils, soybean is the most used raw material in biodiesel production. According to ANP (Brazilian National Agency of Petroleum, Natural Gas and Biofuels), in December 2015, this oil source accounted for 91.47% of the biodiesel produced in Brazil, followed by animal fat (5.58%), cottonseed oil (2.88%), and other fatty materials (0.06%).[2] Soybean oil is also an essential raw material in the United States, with 519 million pounds consumed by June 2016.[3] On the other hand, in Germany, rapeseed oil is the preferred source for biodiesel production.[4]

Unlike fossil fuels, that are relatively inert and retain their essential characteristics during storage, biodiesel degrades with time. Oxidation of biodiesel is a very complex process that can be affected by many factors such as composition of the fuel and storage conditions.[5] The fatty acid profile of biodiesel corresponds to that of parent oil or fat and is a major factor influencing its properties. However, the biodiesel and its blends have been found to be more prone to oxidation than the vegetable oils themselves.

The use of such degraded biofuel in engines causes operational problems like fuel filter plugging, injector fouling, and deposit formation in the engine combustion chamber and in various components of the fuel system, affecting the engine's performance severely.[6,7] The low quality of fuel can be characterized by a series of indicators, such as the appearance of color and the presence of soluble gums and insolubles in the fuel, which are important stability characteristics.[7,8] Changes in the quality of biodiesel as increasing in its acidity (through hydrolysis), oxidation, and the formation of undesirable products (e.g., polymers and deposits) have been studied by several research groups.[5,9−15]

The resistance of biodiesel to oxidative degradation during storage is an important issue concerning both the viability and sustainability of such a class of alternative fuels. Storage stability is the capacity of liquid fuel to resist to changes in its physical and chemical characteristics brought about by its interaction with environment.[16] Various authors have carried out long-term storage tests on biodiesel quality and investigated the effect on the physical properties of the fuel with respect to time.[16−18] According to the results obtained by Das et al.[16] for 180 days storage of biodiesel produced from Karanja oil, the peroxide value and viscosity increased with the increase in the storage time, meaning that the oxidative stability was decreased. Bondioli et al.[17] reported that, after one year of storage,

Received: July 5, 2016
Revised: August 31, 2016

DOI: 10.1021/acs.energyfuels.6b01614
Energy Fuels XXXX, XXX, XXX−XXX

peroxide values increase, but the most significant changes were recorded in oxidation stability, evaluated by Rancimat tests. Bouaid et al.[18] conducted a study for a period of 30 months and observed that the acid value, peroxide value, viscosity, and insoluble impurities increased, while the iodine value decreased, by increasing the storage time of biodiesel samples.

The tendency of adding certain biodiesel content to diesel is growing gradually in Brazil. Currently, the Brazilian commercial diesel corresponds to a B7 (7% biodiesel added to diesel) blend. The law no. 13263 (March 23, 2016)[19] states that, within 12 months, the fraction of biodiesel added to diesel will be 8% (B8), within 24 months, 9% (B9), and within 36 months, 10% (B10). After this period and conducting tests on engines to validate the use of the biodiesel−diesel mixtures, the proportion of biodiesel added to the diesel sold to the Brazilian consumer will be 15% (B15). Recently, the Brazilian government introduced in the national market the low sulfur content diesel (S10). Therefore, the products S500 and S10 (containing not more than 500 mg kg^{-1} and 10 mg kg^{-1} of sulfur, respectively) coexist currently for the road segment.

Infrared spectroscopy (FTIR) is an analytical technique widely used to monitoring the quality of biodiesel/diesel blends, including the checking of fuel adulteration. FTIR has many advantages: it is a nondestructive technique, which allows direct and rapid determination of various properties, without the need of sample pretreatment. The literature reports the use of FTIR to monitoring the transesterification of vegetable oils with methanol[20,21] and ethanol.[22] Several studies have been reported using FTIR for the analysis of free fatty acid.[23−26] This technique has also been used in the determination of the anisidine value.[24,27] Various authors[28−30] have also employed FTIR to determine the degree of unsaturation from mixtures of fatty acids. The progress of the transesterification involving different mixtures of animal fat and soybean oil was monitored by the FTIR absorbance bands at 1465 and 1436 cm^{-1} by Canoira et al.[31]

As diesel and biodiesel have different chemical groups, the infrared spectra of these fuels contain specific characteristic bands; thus, this technique may also be used to quantify the percentage of biodiesel in biodiesel/diesel combinations.[32] The ABNT NBR 15568 standards,[33] ASTM D7371,[34] and DIN EN 14078[35] establish conditions for the quantification of biodiesel in diesel by spectroscopy in the mid-infrared region employing a multivariate calibration model based on the PLSR (partial least squares regression) mathematical algorithm. Hence, this technique represents a quite conventional method to evaluate the percentage of biodiesel in Bx blends.

On the other hand, an attenuated total reflectance (ATR) accessory in FTIR spectroscopy and Raman spectroscopy itself are less used tools considering these determinations, although they allow for fast quantitative analyses and do not require sample preparation, nor the use of any solvent.[36,37] This is completely in line with environmentally friendly Green Chemistry precepts.

In summary, there are abundant publications on the storage and oxidative stability of vegetable oils and biodiesel, although there is still scarce literature available concerning biodiesel/diesel mixtures, mainly about the particular biodiesel Brazilian matrixes (i.e., soybean/tallow). However, maintaining the quality of biodiesel in Bx blends is mandatory with the aim of spreading its use as an alternative source of energy. The degradation of these blends during long storage periods should therefore be the object of study and research, especially in Brazil, taking into account the new national laws regarding the use of low sulfur content S10 diesel in those mixtures. In this context, the present work reports a series of physicochemical studies performed on commercial Bx mixtures constituted of 80/20% soybean/tallow biodiesel in S10 and S500 oil diesel and investigates the performance of two rapid and still underexplored techniques, namely, mid-infrared using a horizontal ATR (HATR) accessory and Raman spectroscopies, to evaluate the hydrolysis and oxidative stability of these blends.

2. MATERIALS AND METHODS

Samples of type A, i.e., biodiesel-free diesel having not more than 500 mg kg^{-1} (S500) and 10 mg kg^{-1} (S10) of sulfur, were provided by Ipiranga Produtos de Petróleo S.A. (Caxias Distribution Center), as characterized by the manufacturer. The product was specified according to the parameters listed in the ANP Technical Regulations 50/2013,[38] 69/2014,[39] and 13/2015,[40] without the addition of any antioxidant agent. The S500 diesel marketed in Brazil receives the addition of an azo dye, namely, Sudan III, to differentiate it from the low sulfur diesel S10, which is colorless to pale yellowish.

100% soybean [50.6% wt linoleic acid (C18:2), 25.3% wt oleic acid (C18:1), 11.4% wt palmitic acid (C16:0), 8.2% wt linolenic acid (C18:3), 4.2% wt stearic acid (C18:0)] biodiesel and 100% bovine/suine tallow [42.2% wt oleic acid (C18:1), 24.6% wt palmitic acid (C16:0), 19.2% wt stearic acid (C18:0), 5.6% wt palmitoleic acid (C16:1), 3.5% wt miristic acid (C14:0)] biodiesel were produced by the methyl route through basic transesterification, without the addition of antioxidants. Characterizations were made by the producing plants, according to the ANP Technical Regulation 45/2014.[41] The biodiesel matrix used in this work was prepared by mixing 80% soybean biodiesel and 20% tallow biodiesel by volume. Biodiesel/diesel blends, on the other hand, were constituted from this biodiesel matrix and S10 or S500 diesel oil in the ratios 0%, 7%, 20%, and 100% of biodiesel by volume. All of the samples were prepared in duplicate and identified as B0 S10 (0% biodiesel by volume in S10 diesel), B0 S500 (0% biodiesel by volume in S500 diesel), B7 S10 (7% biodiesel by volume in S10 diesel), and B7 S500 (7% biodiesel by volume in S500 diesel), B20 S10 (20% biodiesel by volume in S10 diesel), B20 S500 (20% biodiesel by volume in S500 diesel), and B100 (100% soybean/tallow biodiesel). The blends were vigorously homogenized, and volumes of 100 mL were transferred to proper glass vials (borosilicate) with an aperture of 5 mm diameter on its cover to allow the entrance of atmospheric oxygen and oxidation of the samples. A total of 112 flasks representing the seven studied blends were analyzed in duplicate at eight different times (namely, 0, 2, 4, 6, 8, 13, 18, and 24 weeks).

The samples were stored during 24 weeks in an oven set at (43 ± 2) °C[42] and with free air circulation. Periodically, at 2, 4, 6, 8, 13, 18, and 24 weeks, vials were removed and placed in the dark for 30 min to reach room temperature, preventing photolytic reactions, and some stability parameters were evaluated. The homogeneity of the oven temperature and internal moisture were verified through a calibrated thermos hygrometer installed inside the oven, which was programmed to automatically record temperature and moisture once a day for 24 weeks. The 43 °C temperature and storage time of 24 weeks were chosen based on ASTM D4625,[42] which simulates a less stressful fuel storage. A more stressful condition, on the other hand, would be at the temperature of 90 °C, suitable to simulate situations of interest to the automotive industry.[43]

The following analyses were carried out in the studied mixtures at all times, in order to evaluate the degree of sample degradation: oxidative stability by Rancimat (DIN EN 15751[44]), water content by Karl Fischer (ASTM D6304[45]), and Raman and HATR mid-infrared spectroscopies. On the other hand, the acid value tests (ASTM D664[46]), biodiesel content (DIN EN 14078[35]), and elemental analysis by ICP-AES (ASTM D7111[47] and NBR 15553[48]) were only analyzed at the beginning and end of the experiments (points 0 and 24 weeks, respectively).

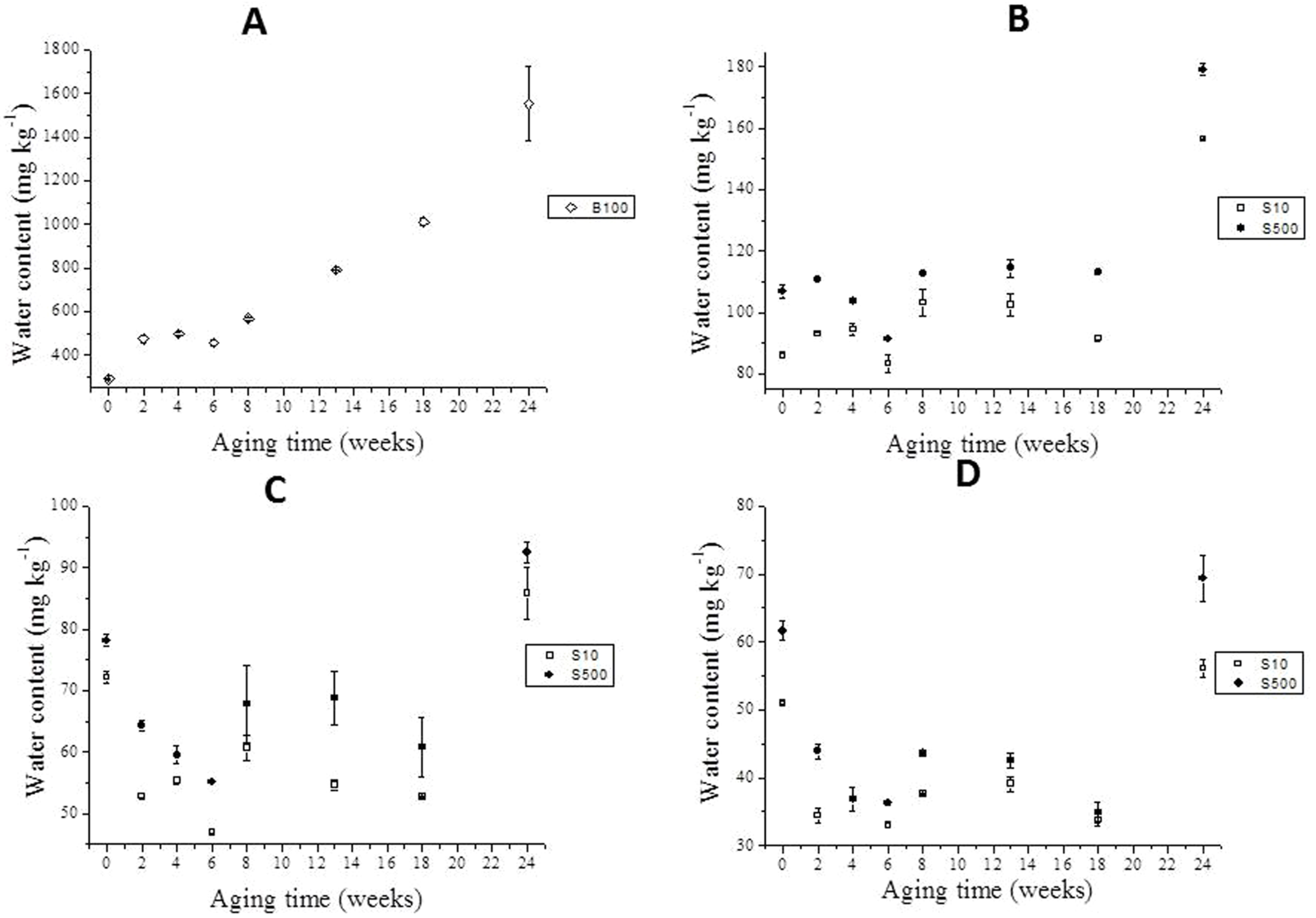

Figure 1. Water content for biofuel (B100) and biofuel/fuel blends (S10 and S500) for the 24 weeks experiment: A: 100% biodiesel (B100); B: 20% biodiesel (B20); C: 7% biodiesel (B7) and D: 0% biodiesel (B0). Error bars are calculated from the standard deviation.

3. INSTRUMENTATION

Water Content. For the determination of water content in the samples, automatic coulometric titrations were carried out, by using a Metrohm KFC apparatus, model 756, coupled to an oven sample processor, following the standard ASTM D6304.[45]

Biodiesel Content. The biodiesel content in diesel was analyzed at the beginning and end of the experiment (t_0 and t_{24}) according to the standard indicated in ANP Technical Regulation 50/2013,[38] which is based on DIN EN 14078[35] (by regular FTIR spectroscopy). The equipment used was a Spectrum 100 mid-infrared PerkinElmer spectrophotometer. The samples B20 and B100 were diluted, respectively, 4 and 20 times in cyclohexane, in order to quantify them in the same analytical curve used for the other samples.

Acid Value. The acid value of fuel samples was determined at the beginning and at the end of the experiments (t_0 and t_{24}) in an automatic 836 titrando equipment (Metrohm, Switzerland), with a combined glass membrane pH electrode saturated with lithium chloride (in ethanol). The acid values of the biodiesel/diesel blends were obtained by the standard test method for acid number determination, based on potentiometric titration, ASTM D664.[46]

ICP-AES. The metals act as catalysts for the decomposition of hydroperoxides, accelerating autoxidation.[49] In this sense, the multielemental content of all the studied blends at t_0 and t_{24} was analyzed by inductively coupled plasma atomic emission spectrometry, ICP-AES, in a Plasma P1000 PerkinElmer apparatus, following ASTM D7111[47] for pure diesel and its blends and ABNT NBR 15553[48] for the B100 samples.

The procedures are based on dilution of samples in a suitable solvent; in this study was used high purity kerosene, from Sigma-Aldrich. The dilution factor used for diesel samples was 2× and 4× for the biodiesel ones, so that the solutions had not much different viscosities and reached the optical detection limit of the method. Yttrium was added as an internal standard, and a standard certificate was used to validate the method, NIST 1084a, which showed the expected recovery.

Oxidative Stability. The oxidative stability was determined using the Rancimat equipment (Metrohm, model 892), according to the European Standard DIN EN 15751.[44] The minimum limit of biodiesel to meet the criteria of this method is 2% by volume, as amounts containing less than this percentage of biodiesel make the test inaccurate due to increased vaporization of the sample, which ends up degrading and evaporating before the period induction can be determined.

Infrared Absorption Spectroscopy. Each sample was evaluated by its infrared absorption spectrum, obtained on a Spectrum 100 FTIR spectrophotometer (PerkinElmer) having a HATR accessory and processed by the 6−1.0 Spectrum software package (PerkinElmer). The spectra were collected at a resolution of 4 cm^{-1}, using a four scan accumulation (recorded from 4000 to 650 cm^{-1}). The ZnSe cell was cleaned two times with small amounts of *n*-heptane before each sample be placed in it, without any kind of pretreatment, as a thin film.

Raman Spectroscopy. Raman scattering spectra were obtained with a FT-Raman spectrometer model Station 400 (PerkinElmer). Samples were placed directly into a quartz cuvette (10 mm optical path length), and the spectra were collected in the wavenumber range (3300−200) cm^{-1} with a resolution of 4 cm^{-1} (four scan accumulation). The laser excitation frequency was 780 nm (red light), its intensity, 100%, and the camera's position in the horizontal CCD detector at −49 °C were as follows: back/forward to 20 mm, left/right to 71 mm, up/down to 0 mm. The spectra were processed

DOI: 10.1021/acs.energyfuels.6b01614
Energy Fuels XXXX, XXX, XXX−XXX

Table 1. Basic Chemical Characterization of Samples: Water Content, Biodiesel Content, and TAN, Carried out at the Beginning (t_0) and at the End (t_{24}) of the Experiments[a]

assays	water content by Karl Fischer (mg kg^{-1})		biodiesel content (% by volume)		TAN (mg KOH g^{-1})	
samples[b]	t_0	t_{24}	t_0	t_{24}	t_0	t_{24}
B100 x	294 ± 13	1671 ± 36	103.6 ± 6.5	106.0 ± 6.7	0.29 ± 0.11	2.29 ± 0.25
B100 y	290 ± 13	1432 ± 33	102.8 ± 6.5	100.6 ± 6.4	0.30 ± 0.11	2.01 ± 0.23
B0 S10 x	51 ± 4	55 ± 5	0.0 ± 0.0	0.0 ± 0.0	0.02 ± 0.04	0.02 ± 0.04
B0 S10 y	51 ± 4	57 ± 5	0.0 ± 0.0	0.0 ± 0.0	0.02 ± 0.04	0.03 ± 0.04
B7 S10 x	72 ± 5	89 ± 6	7.0 ± 0.4	7.5 ± 0.5	0.04 ± 0.05	0.03 ± 0.04
B7 S10 y	73 ± 6	83 ± 6	7.0 ± 0.4	7.5 ± 0.5	0.04 ± 0.05	0.03 ± 0.04
B20 S10 x	86 ± 6	156 ± 9	20.2 ± 1.3	19.6 ± 1.2	0.08 ± 0.06	0.08 ± 0.06
B20 S10 y	86 ± 6	157 ± 9	20.1 ± 1.3	22.4 ± 1.4	0.08 ± 0.06	0.08 ± 0.06
B0 S500 x	63 ± 5	67 ± 5	0.0 ± 0.0	0.0 ± 0.0	0.04 ± 0.05	0.02 ± 0.04
B0 S500 y	61 ± 5	72 ± 6	0.0 ± 0.0	0.0 ± 0.0	0.04 ± 0.05	0.04 ± 0.05
B7 S500 x	79 ± 6	91 ± 6	6.8 ± 0.4	7.3 ± 0.5	0.06 ± 0.06	0.07 ± 0.06
B7 S500 y	78 ± 6	94 ± 6	6.8 ± 0.4	7.5 ± 05	0.06 ± 0.06	0.07 ± 0.06
B20 S500 x	109 ± 7	178 ± 9	19.6 ± 1.2	22.9 ± 1.4	0.10 ± 0.07	0.15 ± 0.08
B20 S500 y	105 ± 7	180 ± 10	19.6 ± 1.2	20.2 ± 1.3	0.10 ± 0.07	0.15 ± 0.08

[a] The respective reproducibility of each standard procedure is included in the results. [b] x and y refer to replicates.

by the Spectrum 6.3.5 software package (PerkinElmer). The *n*-heptane and acetone, used in very small quantities in order to clean and dry the cell, respectively, were purchased from Vetec (Brazil).

4. RESULTS AND DISCUSSION

Water Content. Figure 1 shows the water content measured during the course of experiments. As can be seen, biodiesel samples absorb a great quantity of water. This can be attributed to its high hygroscopy.[50] In this sense, as expected, samples with higher biodiesel content had a greater water increase. At the end of the experiment, the B100 sample showed a growth of 430% in the content of water in comparison to the initial value, while the B20 sample increased its water amount by about 70% and the B7 sample, by only 19%.

As can be observed in Figure 1B, C, and D, the water contents of the blends containing S500 diesel, as well as that of pure S500 diesel itself, are greater than those derived from the S10 fuel, even when comparing samples containing the same biodiesel percentage. This suggests that the absorption of water is a process not only associated with the presence of biodiesel, but to the nature of the diesel used as well. In the process of sulfur components removal from diesel, also polar olefins and aromatics, besides phenolic and amine components, are withdrawn from the fuel, leading to an increase in saturation. This makes the S10 diesel "less polar" and hence reduces its ability to incorporate water. Teixeira and Cortás (unpublished results) have verified the higher affinity for water of the S500 diesel in relation to S10, being this solvent easier to separate from S10 blends.

Chemical Characterization of the Samples. The initial (t_0) and final (t_{24}) water and biodiesel contents, as well as TAN for all of the studied samples, are shown in Table 1.

For the biodiesel content parameter, a paired nonparametric test (the Wilcoxon test),[51] where the samples' average before and after aging (t_0 and t_{24}) shown in Table 1 were statistically compared at a 95% level of confidence, resulted in non-significant differences between both groups since $T_{\text{calculated}}$ (= 7) is smaller than $T_{\text{tabulated}}$ (= 8).

There are two main biodiesel degradation pathways: oxidation and hydrolysis. The acid value is an indicator of the hydrolysis progress. Water hydrolyzes the biodiesel to form free carboxylic acids. In our study, no significant variations in the results of acid value were found between initial and final times neither in all of the blends considered nor in the pure diesel samples. However, the B100 samples showed a significant increase, of about 7 times, in the TAN parameter. These results are in accordance with the literature. For example, El Boulifi et al.[52] observed that the acid value of corn biodiesel increased (about 3-fold) after six months of storage at normal temperature. The difference found in the acidity increment due to storage in the present work can be attributed to the altered storing temperatures to which samples were submitted, as temperature plays a crucial role in biofuel oxidation, and even to the diverse fatty acids' content of the samples compared (corn vs soybean/tallow). It is worth noting that the t_0 TAN values correlate very well with the water content of the samples, as measured by Karl Fischer. This is also true for the acidity of the high biodiesel content samples (B100 and B20), regarding the final, i.e., 24 weeks storage, TAN determinations.

Currently, there is no acidity limit for the use of road diesel in Brazil. However, considering the limit for biodiesel of 0.50 mg KOH g^{-1},[41] it can be concluded that the acidity values determined for the blends would not lead to the reduction of fuel quality, not causing thus problems concerning their use.[53]

The ICP-AES analysis showed the presence of sodium and calcium from biodiesel production, but the values found are lower than the maximum limits for biodiesel stated in ANP Technical Regulation 45/2014.[41] Other metals are present in ultralow (traces) concentrations, most of them being under the method's limit of detection.

Accelerated Oxidative Stability. The accelerated oxidative stability through Rancimat determines the sample's antioxidant reservation. The standard method DIN EN 15751[44] can be applied to both pure biodiesel (B100) samples and to biodiesel/diesel blends, provided they contain, at least, 2% biofuel by volume. Due to this reason, we have not made this analysis to the B0 samples. ANP Technical Regulation 45/2014[41] states that the oxidative stability (Rancimat) for pure biodiesel should be at least 8 h. Meanwhile, ANP Technical Regulation 2/2011[54] imposes a minimum of 20 h to the oxidative stability of B6−B20 mixtures using the standard method DIN EN 15751.[44]

Figure 2 presents the variation on the oxidation stability of blends (S10 and S500) and biofuel (B100) at the beginning (t_0) and the end (t_{24}) of the experiments. B7 blends have higher values than the one specified in ANP Technical Regulation 2/2011,[54] even at the end of the experiment (after 24 weeks of storage at 43 °C), which indicates that these blends are completely within specification. On the other hand, the induction times of the B20 mixtures are smaller than the minimum specified already in the beginning of the experiments. B100 samples exhibited, as soon as after 2 weeks of storage, induction times 27% lower than those at the beginning of the experiment. These t_2 values are below 8 h, being out of ANP Technical Regulation 45/2014 specification.[41] At t_8, i.e., after 8 weeks of storage, the induction period reduced to 0.01 h, thus remaining until the end of the experiments. This may be attributed to two different reasons. First, biodiesel hygroscopy, since water absorbed by the blends hydrolyzes the fatty acid esters in the mixture and therefore contributes to a reduction in the oxidative stability. Induction time data are in agreement with the water content in the samples. Second, and perhaps more important, the greater amount of insaturations in the high biodiesel content samples, as double bonds constitute points readily susceptible to oxidation processes.

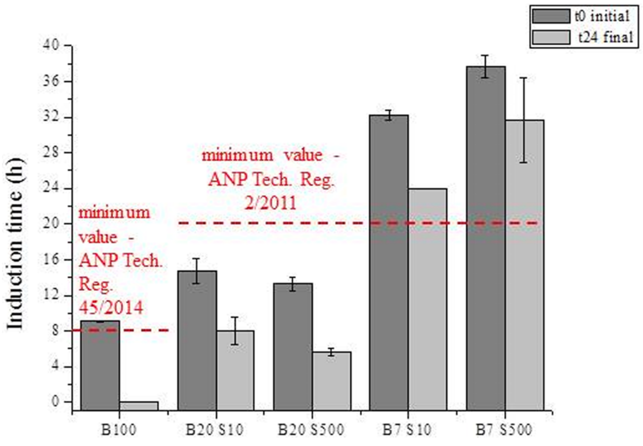

Figure 2. Variation on the oxidation stability of blends (S10 and S500) and biofuel (B100) at the beginning (t_0) and the end (t_{24}) of experiments, with the minimum values specified in ANP's Technical Regulations. Error bars were calculated from the standard deviation.

ASTM D4625 states that each week at 43 °C corresponds to a month of storage at 70 °F.[42] Assuming that we accept this relationship for the studied blends, only B7 mixtures are an acceptable fuel according to ANP Technical Regulation 2/2011.[54]

Although the ASTM D4625[42] test condition of 43 °C may be not suitable for B100 samples (since the test was developed for assessing the stability of petroleum-derived fuels), reactions that occur in diesel-containing blends at typical storage temperatures are apparently the same as those that occur at 43 °C. Bondioli et al.[55] compared the results from D4625 assays upon

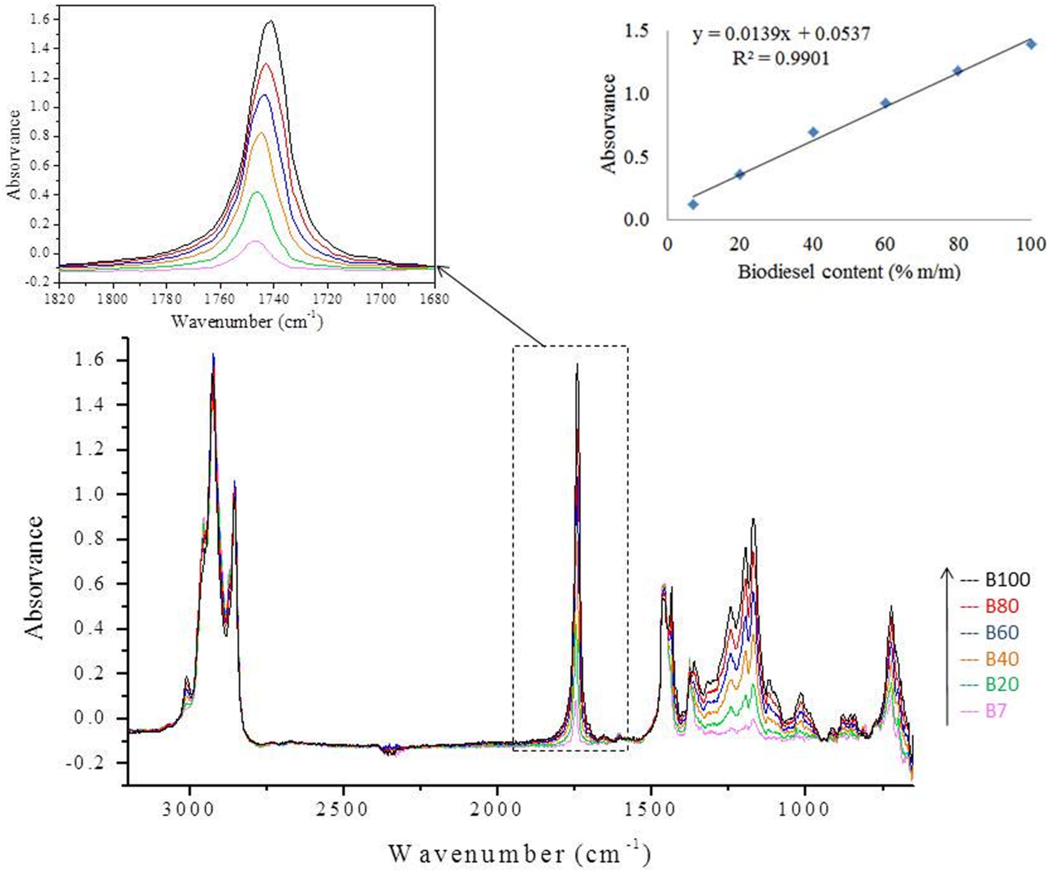

Figure 3. Overlapped spectra in the mid-infrared (FTIR-HATR) of S10 diesel mixtures containing different percentages of biodiesel at t_0. Insets: a detail of the carbonyl ester band (1746 cm^{-1}), selected for analysis (left) and the analytical curve of band intensity as a function of biodiesel content in the blend (right). The profile corresponding to S500 blends is quite similar to the one represented in the figure.

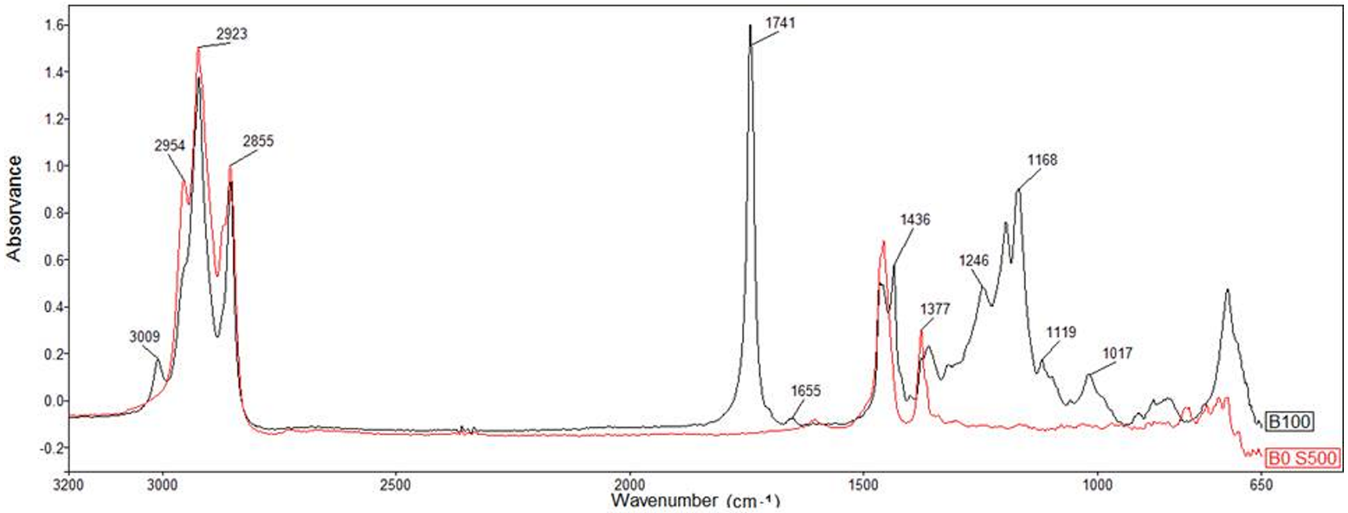

Figure 4. Comparative FTIR-HATR spectra, with main distinctive bands highlighted, of pure biodiesel (B100) and biodiesel-free diesel fuel (B0 S500) before the aging process.

storage for a year in drums at 43 °C and at room conditions. Their results for the room temperature study showed only modest degradation, while in the D4625 temperature (43 °C) experiment the results revealed significant levels of fuel degradation, indicating that deleterious reactions occurring in B100 are accelerated much more by increasing the temperature than those that happen in conventional diesel fuels.

Therefore, the oxidative stability of B7 and B20 blends, independent of the sulfur content of the diesel, is greater than that of B100. The B7 blends have a higher oxidative stability than B20 blends. These results support the clue that biodiesel stability, and not the diesel properties, is the main factor affecting the impact of blends stability on fuel systems and injector deposits and durability.

Infrared HATR Spectroscopy. The mid-infrared spectra of a series of biodiesel/diesel (S10) blends, prepared in order to evaluate the quality of the FTIR-HATR-derived analytical curve, are depicted in Figure 3. All of the measurements were obtained at t_0 (not aging) and constitute the typical biofuel/fuel vibrational profile before oxidation of the samples.

The correlation coefficient of the analytical curve was 0.9901, indicating that the FTIR-HATR technique represents a very good method to quantify esters (and, therefore, biodiesel) in the blends. S10 blends gave the linear equation $y = 0.0139x + 0.0537$, while for S500 blends (not shown in Figure 3) the linear regression was $y = 0.0137x + 0.1204$.

Differences in chemical composition of biodiesel compared to diesel directly impact on fuel properties. Diesel is a petroleum-derived fuel, consisting of paraffinic, naphthenic hydrocarbons, ranging from 10 to 28 carbons.[56] On the other hand, biodiesel is a biofuel consisting of fatty acids methyl or ethyl esters, produced from renewable sources (mainly vegetable oils) using pure alcohol and small amounts of catalyst.[57]

Figure 4 shows the mid-infrared spectra of pure S500 diesel (B0 S500) and pure biodiesel (B100) before aging of the samples. A band present at approximately 3009 cm^{-1} in the B100 spectrum can be assigned to the CH stretching vibrations of cis unsaturations in the esterified fatty acids chains of biodiesel. The asymmetric stretching (2923 cm^{-1}) and the symmetric stretching (2855 cm^{-1}) bands of the methylene groups, as well as a shoulder in the former absorption (2954 cm^{-1}) corresponding to asymmetrical stretchings of the terminal methyl groups can be easily identified in both spectra. The stretching vibration of the ester triglycerides, only present, as expected, in the B100 spectrum, is observed at 1741 cm^{-1}. A low-intensity band is detected at 1655 cm^{-1} and could be attributed to the stretching vibration of C═C bonds of the acyl groups of oleic and linoleic acids present in B100. There is, in B100 and B0 S500 spectra, an asymmetric band at approximately 1436 cm^{-1}, which can be assigned to bending movements of the scissoring type involving methylene groups of the chains. On the other hand, the 1377 cm^{-1} band can be associated with the symmetric bending of methyl groups. The bands at 1246, 1168, 1119, and 1017 cm^{-1}, which are absent in the B0 S500 spectrum, can be assigned to the stretching vibrations of the different esters C—O bonds.[58−61]

As stated above, there are two main biodiesel degradation pathways: oxidation and hydrolysis. The vulnerability of this fuel to oxidation during storage is related to the presence of unsaturations in its fatty acids chains. The kinetics of biodiesel oxidation is highly reliant on both the number of C═C double bonds and their relative positions within the molecule (dioxygen readily reacts with bis-allylic methylene groups, after homolytic scission of a C—H bond, initiating an autoxidation radical chain reaction sequence that leads to hydroperoxides as the first stable products). The overall oxidation stability could also be affected by cis/trans isomerization.[62,63] On the other hand, absorbed water hydrolyzes the biodiesel to form free carboxylic acids, which, in turn, impact on TAN values. In this context, the hygroscopy of biodiesel is a point to be considered.

Bands in the fingerprint region should not be used as a parameter in the evaluation of stability toward degradation, as they are usually overlapped, preventing their isolation in order to quantitatively determine their area or intensity. Consequently, the high intensity band at 1746 cm^{-1} was chosen to evaluate the extension of hydrolysis, even though some bands observed in the fingerprint region have suffered a great variation upon time degradation.

Biofuel samples contain a mixture of several different components, and specific, completely free of interferences, absorptions related to individual constituents/groups are very difficult to find. For this reason, in the present study, the ratio

DOI: 10.1021/acs.energyfuels.6b01614

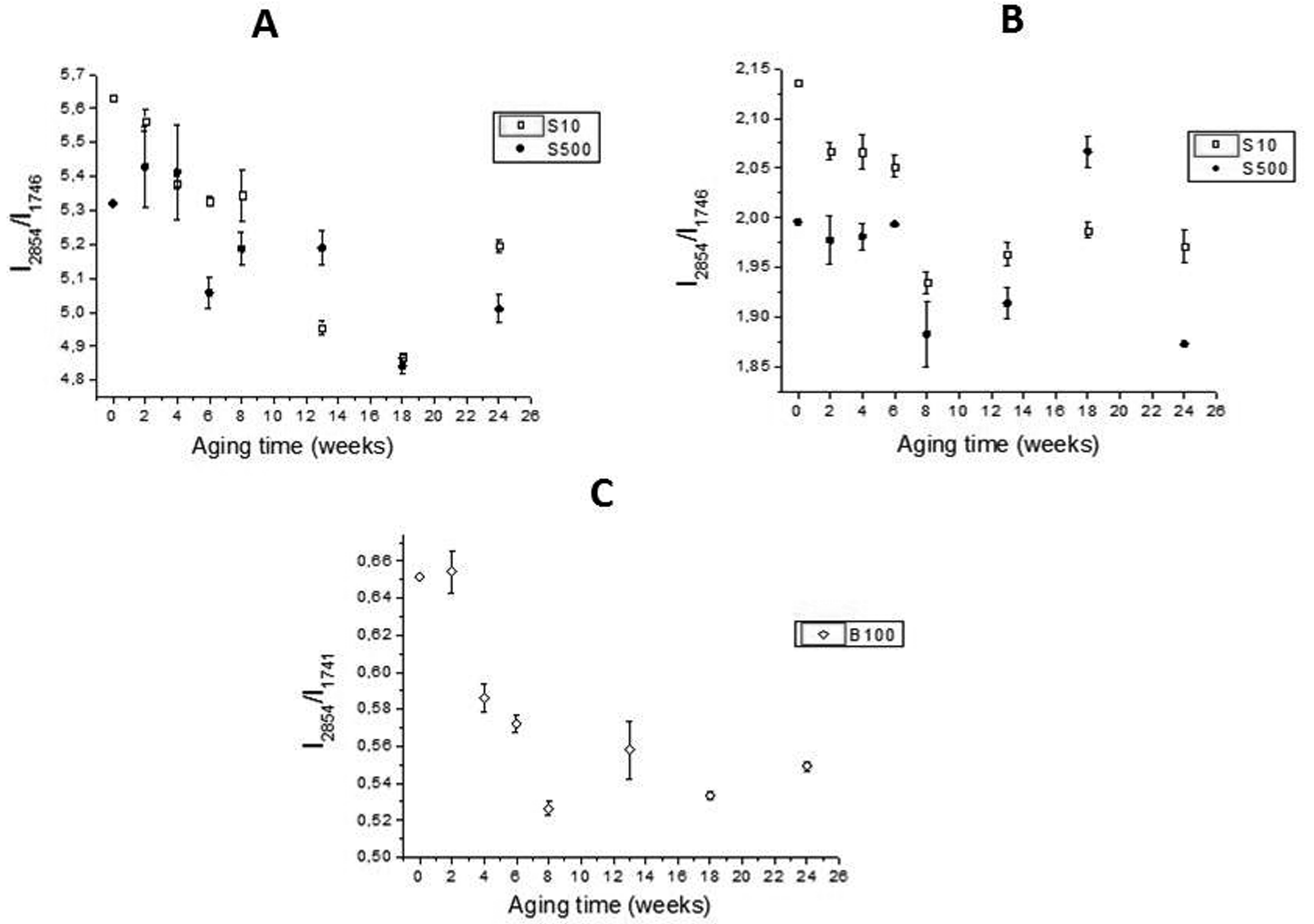

Figure 5. Variation of the I_{2854}/I_{1746} ratio for fuel blends (S10 × S500) and I_{2854}/I_{1741} ratio for pure biofuel maintained at 43 °C. A: 7% biofuel (B7); B: 20% biofuel (B20) and C: 100% biofuel (B100). Error bars calculated from the combined standard deviations.

between the intensities of a reference peak and that of the peak of interest at a given time, i.e., $(I\nu_1/I\nu_2)_{tx}$, were used to monitory sample stability, since this approach minimizes natural variations between replicates and allows for comparison of data recorded on different times. Other authors had already used specific spectral intensity ratios to monitor fuel stability.[64−67] The band at 2854 cm^{-1} was chosen as a reference (ν_1), since it is narrow, relatively symmetrical, and assigned to symmetric stretching of methylene groups, which are expected not to undergo major variations during the aging process.

The band related to the carbonyl stretching of esterified fatty acids, at 1746 cm^{-1}, undergoes noticeable aging-related changes. Figure 5 displays the I_{2854}/I_{1746} ratios over time, along with the respective error bars associated, for the samples B7 (S10 and S500), B20 (S10 and S500), and B100 during the aging experiments. The combined standard deviation for the values of this quotient produced a coefficient of variation of 0.03%.[51]

The I_{2854}/I_{1746}, or I_{2854}/I_{1741} in the case of B100, ratio decreases along aging for all the analyzed samples, meaning that C═O "concentration" is progressively increasing. The effect is definitively larger for B7 blends and is virtually the same for B20 and B100 samples. Secondary oxidation products, such as aldehydes and ketones, absorb near ester carbonyls and may be contributing to an increase in the intensity of this band. Therefore, the decrease in the $I_{2854}/I_{1746\ (1741)}$ ratio can be indicative of the production of secondary oxidation products, which seems to overcome the expected decrease of C═O bonds due to hydrolysis. At the end of the experiments, a reduction of 15.7% was found for the B7 S10 I_{2854}/I_{1746} ratio, while for the B7 S500 sample the reduction was only 10.5%. For the blends with higher biodiesel content, reduction was 7.7% (B20 S10) and 6.2% (B20 S500). As shown by the data above, the relative increase in the C═O band intensity is larger for the blends derived from the low sulfur content diesel. The results obtained for the B7 samples could be rationalized on the basis of both a higher oxidation rate of the B7 S10 blend, since the Rancimat analyses indicated that, in this case, the induction time for B7 S10 is shorter than that of B7 S500, and a reduced rate of hydrolysis, as the S10 diesel is less hygroscopic than S500. On the other hand, for the B20 samples, there is no statistically significant difference between the induction times of B20 S10 and B20 S500, which implies that the dissimilarities observed between these blends are mainly due to hydrolysis (B20 S10 is less hygroscopic and exhibits a diminished hydrolysis rate). This also explains why the impact on the carbonyl band is larger for the B7 blends.

The data can mainly be interpreted as resulting from larger secondary oxidation products formation in the samples. Two concurrent processes, oxidation and hydrolysis, make it unsuitable the use of carbonyl band intensity, measured in the mid-infrared region, as a parameter to accurately quantify fuel degradation.

DOI: 10.1021/acs.energyfuels.6b01614

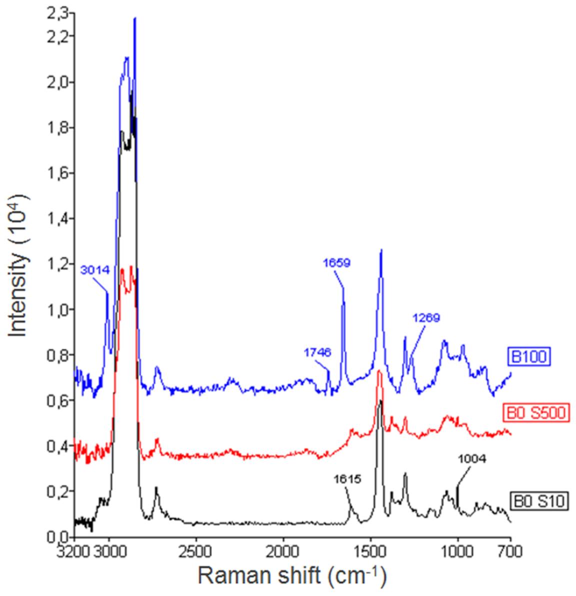

Figure 6. Comparative Raman scattering spectra of pure diesel (B0 S10 and B0 S500) and pure biodiesel (B100) samples, before aging (t_0). Some specific bands are highlighted.

Raman Spectroscopy. Figure 6 displays the Raman spectra of pure diesel (B0 S10 and B0 S500) and pure biodiesel (B100) before the aging process (t_0). Some characteristic bands, which differ from one fuel to the other, are highlighted for the sake of comparison.

The Raman spectrum of pure biodiesel (B100) shows a profile similar to that already reported in the literature.[68] Different from infrared spectroscopy, the carbonyl stretching band observed at 1746 cm^{-1} in the Raman spectrum of B100 is a low-intensity band and, therefore, of limited analytical interest. For this reason, Raman spectroscopy is not the most suitable technique for monitoring the biodiesel hydrolysis reaction.

However, biodiesel has a medium and well-defined band at 1659 cm^{-1}, which is due to the stretching of cis C=C double bonds, molecular point where oxidation takes place. In general, C=C stretching in cis alkenes occurs between (1660 and 1630) cm^{-1}, while C=C stretching in trans alkenes is observed between (1680 and 1665) cm^{-1}. On the other hand, the band associated with the C−H stretching of cis olefins can be observed at 3014 cm^{-1}. This absorption is obviously absent in the diesel spectra.

Figure 7 presents the corresponding calibration plots of the bands at 1659 and 3014 cm^{-1} for biodiesel concentrations ranging from 0% (B0 S10) to 80% by volume, at t_0. The spectrum of pure biodiesel (B100) was not included in order to not radically change the initial analytical matrix (diesel fuel). The correlation coefficient (R^2) values were 0.9944 (absorption at 1659 cm^{-1}) and 0.9868 (band at 3014 cm^{-1}), while the linear regressions afforded, respectively, equations $y = 140.2x + 1159.6$ and $y = 71.355x + 2047.9$. On the other hand, S500 blends (not shown in Figure 8) provided the equations $y = 28.647x + 6847$ ($R^2 = 0.8674$) and $y = 17.17x + 3991.8$ ($R^2 = 0.9197$) for the absorptions at 1659 and 3014 cm^{-1}, respectively. Thus, band intensities correlate well with biodiesel concentrations in the blends, making Raman spectroscopy especially suitable for monitoring the integrity of unsaturations present in the biodiesel chain.

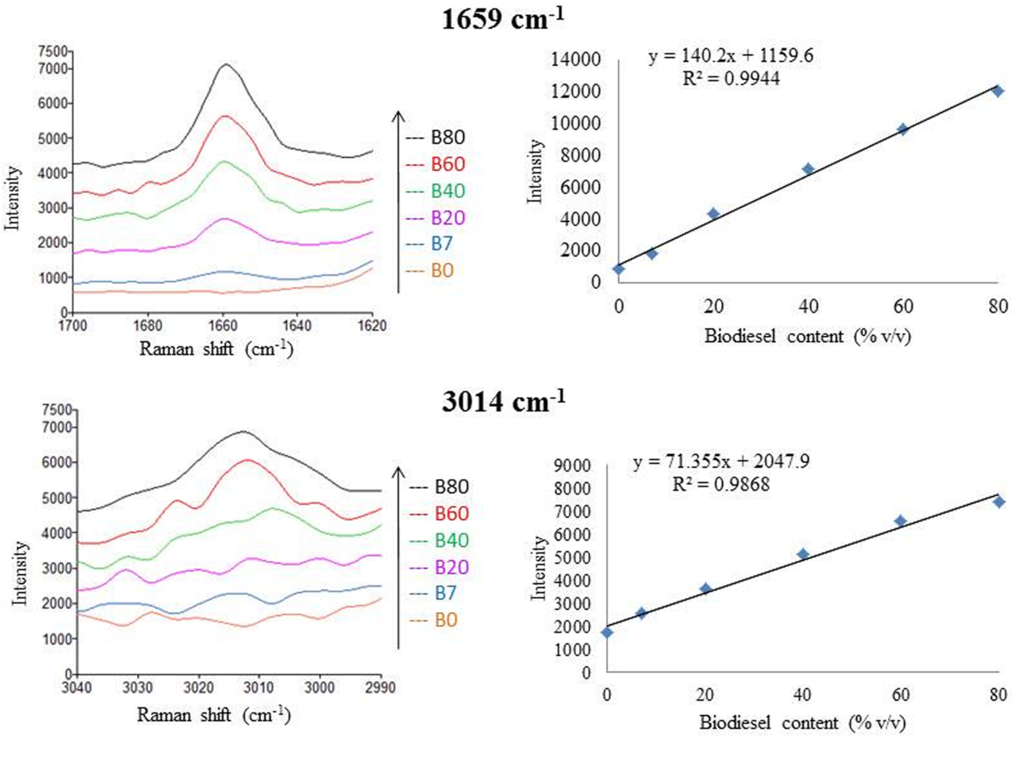

Figure 7. Overlapped Raman spectra (special focus is given to the bands at 1659 and 3014 cm^{-1}) of S10 diesel mixtures containing different percentages of biodiesel, at t_0. The corresponding analytical curves of intensities as a function of biodiesel content in the blend are displayed to the right of each spectrum. The profile corresponding to S500 blends is quite similar to the one represented in the figure.

DOI: 10.1021/acs.energyfuels.6b01614

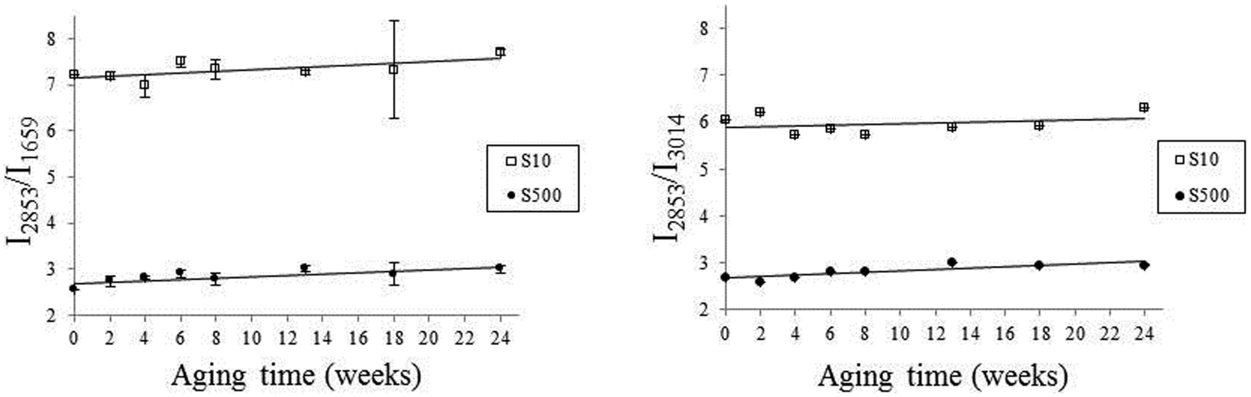

Figure 8. Variation of the Raman intensity ratios I_{2853}/I_{1659} (left) and I_{2853}/I_{3014} (right) for fuel blends (B20 S10 and B20 S500) maintained at 43 °C. Error bars were calculated from the combined standard deviations.

Figure 8 shows the I_{2853}/I_{1659} and I_{2853}/I_{3014} ratios as functions of the aging time for the samples B20 S10 and B20 S500, maintained at 43 °C. B7 blends were not included, since their biodiesel content was too low to allow for accurate quantitative measurements. For samples containing 20% biodiesel, results on the band at 3014 cm^{-1} support the depletion of cis C=C double bonds due to oxidation and/or isomerization. Concerning the I_{2853}/I_{1659} quotient, a similar trend is observed: the increase of the ratio denotes a decrease in the amount of cis C=C double bonds along the aging process.

5. CONCLUSIONS

Biodiesel from sources rich in saturated fatty acids (e.g., tallow) can increase the shelf life of soybean biodiesel. On the other hand, the addition of a certain percentage of biodiesel to diesel, although in line with an environmentally friendly development, affects negatively the aging resistance of the resulting blends.

S500 blends are more acidic then S10 blends, in accordance with the higher water content of the former. At t_0, the acidity of pure (B100) biodiesel (0.50 mg KOH g^{-1}) is much higher than those of S10 (0.02 mg KOH g^{-1}) or S500 (0.04 mg KOH g^{-1}) blends, as B100 is much more hygroscopic than the B7 and B20 mixtures.

Accelerated oxidative stability tests (by Rancimat) showed that the induction times of B7 and B20 samples are greater than that of B100, independent of the sulfur content of the diesel. Among the biodiesel/diesel blends studied, only B7 mixtures are an acceptable fuel according to the ANP Technical Regulation 2/2011.

FTIR-HATR spectroscopy constitute a good analytical tool in order to survey the band at 1746 cm^{-1} (C=O stretching). The practical use of this methodology to characterize Brazilian fuel's degradation stage, however, is conditioned by the fact that there are two main chemical contributions for the band: hydrolysis and oxidation. On the other hand, Raman spectroscopy is not a good technique to follow carbonyl groups, since the resulting bands present very low intensity. Bands at 1659 cm^{-1} (cis alkene C=C stretching) and 3014 cm^{-1} (cis alkene CH stretching), however, represent a very suitable spectroscopic probe for unsaturations in the esterified fatty acids chains of biodiesel.

Since FTIR-HATR and Raman spectroscopies do not require sample preparation, are fast and quite low cost techniques, and cause less impact to the environment than other common methodologies, further attention may be paid to the combination of IR/Raman-derived information in order to separate individual contributions to the main bands, cleaning the way toward the development of high-quality sustainable fuels.

■ AUTHOR INFORMATION

Corresponding Author

*E-mail: nicoarey@puc-rio.br. Phone number: +55 21 3527-1813. Fax: +55 21 3527-1801.

Notes

The authors declare no competing financial interest.

■ ACKNOWLEDGMENTS

V.S.B. Valente would like to thank Ipiranga Produtos de Petróleo S.A. for support and VRAC/PUC-Rio for the conceded scholarship. N.A. Rey would like to thank Brazilian funding agencies FAPERJ (Fundação Carlos Chagas Filho de Amparo à Pesquisa do Estado do Rio de Janeiro) and CNPq (Conselho Nacional de Desenvolvimento Científico Tecnológico) for the research fellowships awarded. The authors acknowledge LABIO/PUC-Rio, LEEA/PUC-Rio, and CTAQ/IPIRANGA for the use of the analytical facilities.

■ ABBREVIATIONS

TAN = total acid number
ICP-AES = inductively coupled plasma atomic emission spectrometry
ASTM = American Society for Testing and Materials
EN = European normalization
ABNT NBR = Brazilian Association of Technical Standards

■ REFERENCES

(1) Saluja, R. K.; Kumar, V.; Sham, R. Stability of biodiesel—A review. *Renewable Sustainable Energy Rev.* **2016**, *62*, 866–881.

(2) ANP, B. M. d. B. Boletim Mensal do Biodiesel da ANP - Agência Nacional do Petróleo, Gás Natural e Biocombustíveis. http://www.anp.gov.br/?pg=69299&m=&t1=&t2=&t3=&t4=&ar=&ps=&1461690233498 (accessed Jan 2016).

(3) Administration, U. S. E. I. www.eia.gov/biofuels/biodiesel/production/biodiesel.pdf (accessed Aug 31, 2016).

(4) Ferrari, R. A.; Oliveira, V. d. S.; Scabio, A. Biodiesel de soja—taxa de conversão em ésteres etílicos, caracterização físico-química e consumo em gerador de energia. *Quim. Nova* **2005**, *28* (1), 19–23.

(5) Knothe, G. Some aspects of biodiesel oxidative stability. *Fuel Process. Technol.* **2007**, *88* (7), 669–677.

(6) Van Gerpen, J. H.; Hammond, E. G.; Yu, L.; Monyem, A. Determining the influence of contaminants on biodiesel properties. *SAE Tech. Pap. Ser.* **1997**, 971685.

(7) Yamane, K.; Kawasaki, K.; Sone, K.; Hara, T.; Prakoso, T. Oxidation stability of biodiesel and its effects on diesel combustion and emission characteristics. *Int. J. Engine Res.* **2007**, *8* (3), 307−319.

(8) Dunn, R. O. Effect of temperature on the oil stability index (OSI) of biodiesel. *Energy Fuels* **2008**, *22* (1), 657−662.

(9) Du Plessis, L.; De Villiers, J.; Van der Walt, W. Stability studies on methyl and ethyl fatty acid esters of sunflowerseed oil. *J. Am. Oil Chem. Soc.* **1985**, *62* (4), 748−752.

(10) Mittelbach, M.; Schober, S. The influence of antioxidants on the oxidation stability of biodiesel. *J. Am. Oil Chem. Soc.* **2003**, *80* (8), 817−823.

(11) Knothe, G.; Dunn, R. O. Dependence of oil stability index of fatty compounds on their structure and concentration and presence of metals. *J. Am. Oil Chem. Soc.* **2003**, *80* (10), 1021−1026.

(12) Polavka, J.; Paligová, J.; Cvengroš, J.; Simon, P. Oxidation stability of methyl esters studied by differential thermal analysis and Rancimat. *J. Am. Oil Chem. Soc.* **2005**, *82* (7), 519−524.

(13) Knothe, G. Analyzing biodiesel: standards and other methods. *J. Am. Oil Chem. Soc.* **2006**, *83* (10), 823−833.

(14) Gonzaga, F. B.; Pasquini, C. A new method for determination of the oxidative stability of edible oils at frying temperatures using near infrared emission spectroscopy. *Anal. Chim. Acta* **2006**, *570* (1), 129−135.

(15) McCormick, R.; Ratcliff, M.; Moens, L.; Lawrence, R. Several factors affecting the stability of biodiesel in standard accelerated tests. *Fuel Process. Technol.* **2007**, *88* (7), 651−657.

(16) Das, L.; Bora, D. K.; Pradhan, S.; Naik, M. K.; Naik, S. Long-term storage stability of biodiesel produced from Karanja oil. *Fuel* **2009**, *88* (11), 2315−2318.

(17) Bondioli, P.; Gasparoli, A.; Della Bella, L.; Tagliabue, S.; Toso, G. Biodiesel stability under commercial storage conditions over one year. *Eur. J. Lipid Sci. Technol.* **2003**, *105* (12), 735−741.

(18) Bouaid, A.; Martinez, M.; Aracil, J. Long storage stability of biodiesel from vegetable and used frying oils. *Fuel* **2007**, *86* (16), 2596−2602.

(19) 13.263, L. d. P. d. R. n., Lei da Presidência da República no. 13.263 de 23 de março de 2016, Diário Oficial da União de 24 de março 2016.

(20) Knothe, G. Rapid monitoring of transesterification and assessing biodiesel fuel quality by near-infrared spectroscopy using a fiber-optic probe. *J. Am. Oil Chem. Soc.* **1999**, *76* (7), 795−800.

(21) Knothe, G. Monitoring a progressing transesterification reaction by fiber-optic near infrared spectroscopy with correlation to 1H nuclear magnetic resonance spectroscopy. *J. Am. Oil Chem. Soc.* **2000**, *77* (5), 489−493.

(22) Zagonel, G. F.; Peralta-Zamora, P.; Ramos, L. P. Multivariate monitoring of soybean oil ethanolysis by FTIR. *Talanta* **2004**, *63* (4), 1021−1025.

(23) Ismail, A.; Van de Voort, F.; Emo, G.; Sedman, J. Rapid quantitative determination of free fatty acids in fats and oils by Fourier transform infrared spectroscopy. *J. Am. Oil Chem. Soc.* **1993**, *70* (4), 335−341.

(24) Dubois, J.; Van de Voort, F.; Sedman, J.; Ismail, A.; Ramaswamy, H. Quantitative Fourier transform infrared analysis for anisidine value and aldehydes in thermally stressed oils. *J. Am. Oil Chem. Soc.* **1996**, *73* (6), 787−794.

(25) Al-Alawi, A.; van de Voort, F. R.; Sedman, J. New FTIR method for the determination of FFA in oils. *J. Am. Oil Chem. Soc.* **2004**, *81* (5), 441−446.

(26) Al-Alawi, A.; van de Voort, F. R.; Sedman, J.; Ghetler, A. Automated FTIR analysis of free fatty acids or moisture in edible oils. *JALA* **2006**, *11* (1), 23−29.

(27) Man, Y. C.; Setiowaty, G. Determination of anisidine value in thermally oxidized palm olein by fourier transform infrared spectroscopy. *J. Am. Oil Chem. Soc.* **1999**, *76* (2), 243−247.

(28) Hendl, O.; Howell, J.; Lowery, J.; Jones, W. A rapid and simple method for the determination of iodine values using derivative Fourier transform infrared measurements. *Anal. Chim. Acta* **2001**, *427* (1), 75−81.

(29) Man, Y. C.; Setiowaty, G.; Van de Voort, F. Determination of iodine value of palm oil by Fourier transform infrared spectroscopy. *J. Am. Oil Chem. Soc.* **1999**, *76* (6), 693−699.

(30) Muniategui, S.; Paseiro, P.; Simal, J. Medida del grado de insaturación de aceites y grasas comestibles por espectroscopia infrarroja y su relación con el índice de yodo. *Grasas Aceites* **1992**, *43*, 1−5.

(31) Canoira, L.; Rodríguez-Gamero, M.; Querol, E.; Alcántara, R.; Lapuerta, M. n.; Oliva, F. n. Biodiesel from low-grade animal fat: production process assessment and biodiesel properties characterization. *Ind. Eng. Chem. Res.* **2008**, *47* (21), 7997−8004.

(32) Guarieiro, L. L. N.; Pinto, A. C.; Aguiar, P. F. d.; Ribeiro, N. M. Metodologia analítica para quantificar o teor de biodiesel na mistura biodiesel: diesel utilizando espectroscopia na região do infravermelho. *Quim. Nova* **2008**, *31* (2), 421−426.

(33) ABNT NBR 15568:2008 Brazilian Standard, *Biodiesel - Determination of biodiesel content in diesel oil via mid-infrared spectroscopy*; Brazilian Association of Technical Standards, Rio de Janeiro, 2008; www.abnt.org.br.

(34) ASTM D7371:2007. *Standard test method for the determination of biodiesel (fatty acid methyl esters) content in diesel fuel oil using mid-infrared spectroscopy (FTIR-ATR-PLS method)*; ASTM International: West Conshohocken, PA, 2007.

(35) Standard DIN EN 14078:2014. *Liquid petroleum products − Determination of fatty acid methyl ester (FAME) content in middle distillates − Infrared spectrometry method*; 2014.

(36) de Souza, A. V. A.; Cajaiba da Silva, J. o. F. Biodiesel Synthesis Evaluated by Using Real-Time ATR-FTIR. *Org. Process Res. Dev.* **2013**, *17* (1), 127−132.

(37) Ghesti, G. F.; de Macedo, J. L.; Resck, I. S.; Dias, J. A.; Dias, S. C. L. FT-Raman spectroscopy quantification of biodiesel in a progressive soybean oil transesterification reaction and its correlation with 1H NMR spectroscopy methods. *Energy Fuels* **2007**, *21* (5), 2475−2480.

(38) *ANP Technical Regulation no. 50* of 23 December 2013, DOU of 24 December 2013.

(39) *ANP Technical Regulation no. 69* of 23 December 2014, DOU of 24 December 2014.

(40) *ANP Technical Regulation no. 13* of 06 March 2015, DOU of 09 March 2015.

(41) *ANP Technical Regulation no. 45* of 25 August 2014, DOU of 26 August 2014.

(42) ASTM D4625:2009. *Standard Test Method for Middle Distillate Fuel Storage Stability at 43 °C (110 °F)*; ASTM International: West Conshohocken, PA, 2009.

(43) Mushrush, G. W.; Beal, E. J.; Hardy, D. R.; Hughes, J. M.; Wynne, J. H. Fuel Instability Studies: The Chemical Validation of ASTM Method D5304. *Pet. Sci. Technol.* **2001**, *19* (5−6), 561−572.

(44) DIN EN 15751:2014. *Automotive fuels − fatty acid methyl ester (FAME) fuel and blends with diesel fuel − Determination of oxidation stability by accelerated oxidation method*; 2014.

(45) ASTM D6304:2007. *Standard Test Method for Determination of Water in Petroleum Products, Lubricating Oils, and Additives by Coulometric Karl Fischer Titration*; 2007.

(46) ASTM D664:2011. *Standard test method for acid number of petroleum products by potentiometric titration*; 2011.

(47) ASTM D7111:2015. *Standard Test Method for Determination of Trace Elements in Middle Distillate Fuels by Inductively Coupled Plasma Atomic Emission Spectrometry (ICP-AES)*;2015.

(48) ABNT NBR 15553:2015. *Biodiesel - Determinação dos teores de cálcio, magnésio, sódio, fósforo e potássio por espectrometria de emissão ótica com plasma indutivamente acoplado (ICPOES)*; Associação Brasileira de Normas Técnicas: Rio de Janeiro, 2015; www.abnt.org.br.

(49) Kamal-Eldin, A.; Pokorny, J. Lipid oxidation products and methods used for their analysis. *Analysis of lipid oxidation. Champaign: AOCS* **2005**, DOI: 10.1201/9781439822395.ch1.

(50) Fregolente, P. B. L.; Fregolente, L. V.; Wolf Maciel, M. R. Water content in biodiesel, diesel, and biodiesel−diesel blends. *J. Chem. Eng. Data* **2012**, *57* (6), 1817−1821.

(51) Miller, J. N.; Miller, J. C. *Statistics and chemometrics for analytical chemistry*; Pearson Education, 2005.

(52) El Boulifi, N.; Bouaid, A.; Martinez, M.; Aracil, J. Process optimization for biodiesel production from corn oil and its oxidative stability. *Int. J. Chem. Eng.* **2010**, *2010*, 1.

(53) Carvalho, R. A. *Estudo da Adição de Biodiesel no Diesel S10 e S500 e seus Efeitos nas Propriedades do Combustível e na Atomização*. Universidade Federal do Rio de Janeiro, 2015.

(54) *ANP Technical Regulation no. 2* of 12 January 2011, DOU of 13 January 2011, rectified in the DOU 03 February 2011.

(55) Bondioli, P.; Gasparoli, A.; Della Bella, L.; Tagliabue, S.; Lacoste, F.; Lagardere, L. The prediction of biodiesel storage stability. Proposal for a quick test. *Eur. J. Lipid Sci. Technol.* **2004**, *106* (12), 822−830.

(56) Brasil, N. I. A.; Araujo, M. A.; Sousa, E. C. M. *Processamento de petróleo e gás*; 2012.

(57) Knothe, G.; Gerpen, J.; Krahl, J.; Ramos, L. *Manual de Biodiesel Edgard Blücher*; São Paulo, 2006.

(58) Guillén, M. D.; Cabo, N. Infrared spectroscopy in the study of edible oils and fats. *J. Sci. Food Agric.* **1997**, *75* (1), 1−11.

(59) Van de Voort, F.; Ismail, A.; Sedman, J. A rapid, automated method for the determination ofcis andtrans content of fats and oils by fourier transform infrared spectroscopy. *J. Am. Oil Chem. Soc.* **1995**, *72* (8), 873−880.

(60) Safar, M.; Bertrand, D.; Robert, P.; Devaux, M.; Genot, C. Characterization of edible oils, butters and margarines by Fourier transform infrared spectroscopy with attenuated total reflectance. *J. Am. Oil Chem. Soc.* **1994**, *71* (4), 371−377.

(61) Guillén, M. D.; Cabo, N. Some of the most significant changes in the Fourier transform infrared spectra of edible oils under oxidative conditions. *J. Sci. Food Agric.* **2000**, *80* (14), 2028−2036.

(62) Osawa, W.; Sahoo, P.; Onyari, J.; Mulaa, F. Effects of antioxidants on oxidation and storage stability of Croton megalocarpus biodiesel. *Int. J. Energy Environ. Eng.* **2016**, *7*, 85−91.

(63) Schneider, C. An update on products and mechanisms of lipid peroxidation. *Mol. Nutr. Food Res.* **2009**, *53* (3), 315−321.

(64) Arnold, R.; Hartung, T. Infrared spectroscopic determination of degree of unsaturation of fats and oils. *J. Food Sci.* **1971**, *36* (1), 166−168.

(65) Afran, A.; Newbery, J. Analysis of the degree of unsaturation in edible oils by Fourier transform-infrared/attenuated total reflectance spectroscopy. *Spectroscopy* **1991**, *6* (1), 31−34.

(66) Moreno, M. M.; Olivares, D. M.; Lopez, F. A.; Adelantado, J. G.; Reig, F. B. Determination of unsaturation grade and trans isomers generated during thermal oxidation of edible oils and fats by FTIR. *J. Mol. Struct.* **1999**, *482*, 551−556.

(67) Guillen, M.; Cabo, N. Characterization of edible oils and lard by Fourier transform infrared spectroscopy. Relationships between composition and frequency of concrete bands in the fingerprint region. *J. Am. Oil Chem. Soc.* **1997**, *74* (10), 1281−1286.

(68) Oliveira, F. C.; Brandao, C. R.; Ramalho, H. F.; da Costa, L. A.; Suarez, P. A.; Rubim, J. C. Adulteration of diesel/biodiesel blends by vegetable oil as determined by Fourier transform (FT) near infrared spectrometry and FT-Raman spectroscopy. *Anal. Chim. Acta* **2007**, *587* (2), 194−199.